Enhanced ciprofloxacin removal from aqueous solution using a chemically modified biochar derived from bamboo sawdust: Adsorption process optimization with response surface methodology

Wondimu K. Wakejo [a, b, *], Beteley T. Meshasha [a, c], Joon W. Kang [c], Jonas Chebude[a,d],

[a] Africa Center of Excellence for Water Management, Addis Ababa University, Addis Ababa, Ethiopia, P.O.Box.1176
[b] Department of Chemical Engineering, Wachemo University, Hossana, Ethiopia, P.O.Box 667
[c] School of Chemical and Bio Engineering, Addis Ababa institute of Technology, Addis Ababa, Ethiopia
[d] Department of Chemistry, College of Natural and Computational Science, Addis Ababa University, Addis Ababa, Ethiopia

[*] Corresponding author. E-mail: wondimu.kebede@aau.edu.et

Abstract

Contamination of water by ciprofloxacin has become a significant concern due to its adverse health effects and growing evidence of antimicrobial-resistant genes evolution. To this end, a chemically modified bamboo biochar was prepared from bamboo sawdust to effectively remove ciprofloxacin (CIP) from an aqueous solution. Under similar adsorption conditions, the modified bamboo biochar (MBC) has an excellent CIP removal efficiency (96%) compared to unmodified bamboo biochar (UBC) efficiency (45%). Thus, MBC was used in batch adsorption experiments and the process was optimized with the central composite design (CCD) framework of response surface methodology (RSM). Sorption process parameters such as initial CIP concentration, pH, adsorbent dose, and contact time were studied and found to have a significant effect on CIP removal. The optimal CIP removal (96%) was obtained at MBC dose (0.5 g L^{-1}), CIP initial concentration (20 mg L^{-1}), pH (7.5), and contact time (46 min). The adsorption kinetic data were well described by the pseudo-second-order model (R^2 = 0.999), and both Langmuir (R^2 = 0.994) and Freundlich (R^2 = 0.972) models gave the best fit in CIP adsorption isotherm analysis. The maximum monolayer adsorption capacity of the MBC was 78.43 mg g^{-1} based on the Langmuir isotherm model. These results suggest that CIP adsorption was mainly controlled by chemisorption. Moreover, the CIP adsorption process was endothermic and spontaneous. Overall, MBC is a low-cost, efficient, and recyclable adsorbent for eliminating emerging contaminants such as ciprofloxacin from an aqueous solution.

1. Introduction

Emerging water contaminants such as pharmaceuticals have recently gained considerable research attention (Balarak et al., 2021). Among pharmaceuticals, antibiotics are the most widely consumed pharmaceutical drugs (Azizi, 2020) that pollute water bodies. There are different classes of antibiotics based on their mechanism of action, chemical structure, action spectrum, and route of administration (Ilurdoz et al., 2022). The most common classification of antibiotics is based on their mode of action, which includes fluoroquinolones, quinolones, β-lactams, sulfonamides, monobactams, carbapenems, and aminoglycosides. Quinolones (ciprofloxacin, levofloxacin, norfloxacin, and ofloxacin) are broad-spectrum antibiotics that are widely prescribed (Ilurdoz et al., 2022). More importantly, CIP stands in the first place based on the number of antibiotics prescribed in this group (Movasaghi et al., 2019). Ciprofloxacin (CIP), a second-generation fluoroquinolone antibiotic, was developed by a German businessman in 1983. It has a fluorine atom at position 6 in the quinolone group to target most gram-negative and some gram-positive bacteria (Falyouna et al., 2022). CIP prevents the replication of bacteria and ultimately inhibits their proliferation (Adaobi et al., 2021). Due to its wide consumption as a broad-spectrum drug (Ilurdoz et al., 2022), incomplete metabolism(15-20%) in humans and animals (Movasaghi et al., 2019; Laurent et al., 2000), higher environmental concentration (up to 20,321 ng L^{-1}) and frequent detection in the environment (Ilurdoz et al., 2022)(Movasaghi et al., 2019; J. Li et al., 2018). CIP has become one of the top priority water contaminants that needs research intervention. It has been released into the environment and detected in groundwater, surface water, and wastewater treatment plant effluents (Yousefi et al., 2021). Antibiotic pollution of ecosystems can pose serious health risks to humans due to their high toxicity and carcinogenic properties (Abu Rumman et al., 2021). Contamination of drinking water supplies with CIP, in particular, can result in serious health effects such as thrombocytopenia, acute renal failure, eosinophilia, elevation of liver enzymes, and leucopenia (Balarak & Mckay, 2021). Albeit low concentration, CIP can promote and accelerate the growth of antimicrobial-resistant (AMRs) genes in water (Falyouna et al., 2022). Therefore, the removal of CIP from an aqueous environment has become an urgent issue (Li et al., 2018).

Conventional wastewater treatment methods are unable to sufficiently remove CIP from water, owing to CIP's biodegradation resistance (Ghadiri et al., 2020; Liang et al., 2018). In response to this problem, removal mechanisms such as ozonation (Bilal et al., 2021), catalytic oxidation (Nemati et al., 2019), photocatalytic degradation of CIP with hematite (Fe_2O_3) nanoparticles (Rajiv et al., 2021), electro-Fenton (Mi et al., 2018), electrocoagulation (Mohammed et al., 2021), magnetic nanomaterials (Chang et al., 2021) reverse osmosis (Río-gamero et al., 2018), solar photo-oxidation (Tawfik et al., 2022) and adsorption (Liang et al., 2018; Río-gamero et al., 2018; Ezekoye et al., 2020) have been explored for the removal of CIP from water. Among the advanced oxidation processes mentioned above, solar photo-oxidation is recently considered a promising way of degrading recalcitrant pollutants in industrial wastewater. Solar energy based water treatment processes are regarded as a sustainable way of pollutants remediation with promising potential (Tawfik et al., 2022). Recently, photocatalytic degradation has been employed for the removal of recalcitrant water contaminants such as norfloxacin (Kumar et al., 2019), ampicillin (Sharma et al., 2018), and methylene blue dye (Sadiq et al., 2021) and showed promising efficiency. However, most of the treatment methods cited above have the issue of efficiency, high energy requirement, generation of toxic by-products, and high treatment cost (Al et al., 2021; Balarak et al., 2021). Therefore, efficient and low-cost treatment options that do not introduce harmful by-products are required to eliminate antibiotics from water (Balarak et al., 2021). In this regard, adsorption is a promising method that achieves these noted benefits, plus it can be implemented without difficulty (Kaya et al., 2021; Ji et al., 2021; Wan and Li, 2019; Al et al., 2021).

Various adsorbents such as montmorillonite (Wu et al., 2010), clinoptilolite (Ngeno et al., 2019), metal-organic framework (Gadipelly et al., 2018), graphene hydrogel (Yu et al., 2019), activated bentonite (Maged, 2020), iron oxide nanoparticle (Lin and Lee, 2020), titanate nanotubes (Ji et al., 2021), silica-xerogels (Kaya et al., 2021), nanocomposite (Elessawy et al., 2020), chitosan (Nazraz et al., 2019) and biochar (Luo et al., 2019; Li et al., 2018; Huang et al., 2018) have been applied for CIP removal. Magnetic nanoparticles such as magnetic core-shell $MnFe_2O_4@TiO_2$ nanoparticles (Chang et al., 2021), humic acid, and levulinic acid-coated Fe_3O_4 nanoparticles are efficient in removing CIP from water (Mahmoud et al., 2021). Other non-magnetic nanoparticles such as graphene oxide nanoparticles were also reported to be efficient for the removal of antidiabetic pharmaceutical (metformin) from an aqueous solution (Balasubramani et al., 2020). However, most of these

adsorbents are associated with complicated preparation techniques, sustainability problems, low CIP uptake (Ezekoye et al., 2020), availability, and higher preparation cost. Despite the promising potential of nanoadsorbents, issues related to separation challenges from aqueous solutions and the associated secondary pollution limited their large-scale applications. As a result, the quest for more cost-effective and efficient adsorbents is ongoing (Ezekoye et al., 2020). Among the adsorbents proposed for CIP removal, biochar has several advantages because of its sustainability, low-cost, feedstock availability and easy separation from aqueous solution (Zheng et al., 2021). On the other hand, transforming low value biomass waste material into value-added materials such as biochar is an example of promoting the circular economy (Osman et al., 2019).

The type and availability of functional groups on the surface of biochar play a critical role in removing pollutants (Kazemi et al., 2020). The high surface area, high mineral content, and sufficient oxygen-containing groups of biochar tend to favor the adsorption of water contaminants (Zheng et al., 2021). Most importantly, chemical modification techniques can easily improve the surface of the biochar. Osman et al. (2020) reported surface areas of 1368 m^2 g and 1142 m^2 g after one step (H_3PO_4) and two steps (H_3PO_4 + KOH) chemical activation of herbaceous lignocellulosic biomass with a surface area of 17 m^2 g before activation.

The adsorptive capacity of the biochar can be enhanced by employing different methods such as chemical modification, physical modification, impregnating with mineral sorbents, and magnetic modification. These modifications can alter the physico-chemical and surface nature of biochars. Compared with physical modification, chemical activation enhances the surface area due to the shorter activation time and lower activation energy of functionalized porous carbons in the presence of an alkaline activation agent (Zheng et al., 2021). Generally, chemical modification of biochar is done via the addition of acids or bases to alter the surface functional properties of the biochar before or after carbonation. Acid activation results in surface acidities and modification of the porous structure of biochar. More often, phosphoric (H_3PO_4), sulphuric (H_2SO_4), nitric (HNO_3), and hydrochloric (HCl) acids (Rajapaksha et al., 2019) are used for acid activation, which yielded improved adsorption capacity. Biochar modified by H_2SO_4, KOH and methanol has shown enhanced tetracycline (TC) removal through π - π EDA interactions because of the functional groups on its surface (Rajapaksha et al., 2019). Alternatively, impregnation with $FeCl_3$, Fe_2O_3, Fe

$(NO_3)_3$, and $MgCl_2$ is performed by soaking biochars or their feedstock in metal nitrates or chlorides solution (Rajapaksha et al., 2019).

Adsorbent preparation using iron salts has the advantages of inducing magnetic properties to the adsorbent for easy separation and enhancing the sorption capacity of the adsorbent by providing additional sorption sites for the removal of the contaminants (Chen et al., 2011; Zhao et al., 2018; Chen et al., 2019; Reguyal et al., 2016). It has been reported that magnetic biochar has demonstrated higher sorption capability for organic pollutants removal compared to non-magnetic biochar (Chen et al., 2011). The higher adsorptive capacity of a magnetic sorbent is probably due to the involvement of Fe-O in the adsorption process (Lim et al., 2009). On the other hand, the alkaline modification of biochar may change the biochar's physical/chemical properties (surface area, pore size, types of functional groups). Li et al. (2017) reported that the KOH treated biochar possessed more mesopores than the raw biochar and showed higher adsorptive performance than the raw biochar (Li et al., 2017). Until now, amine-functionalized bamboo biochar (Peng et al., 2018), bamboo biochar modified with H_3PO_4 and K_2CO_3 (Wang et al., 2015), co-pyrolyzed bamboo and sewage sludge char (Li et al., 2020a) have been investigated for CIP adsorption. However, most of these modification processes involve multi-step processes for biochar preparation. As a result, a simple protocol for producing biochar with a high adsorptive capacity can provide a viable alternative for CIP removal from water. To the best of our knowledge, simultaneous treatment of bamboo sawdust with $FeCl_3$ and KOH for CIP removal from water has not been reported yet.

Bamboo is a plentiful and fast-growing renewable woody plant used in construction and furniture applications. During the technological processing of bamboo for various applications, a considerable amount of bamboo sawdust is generated. Also, it is reported that bamboo waste (BW) has high organic matter content (Li et al., 2020). Due to its low-cost and availability, this study considered bamboo sawdust for CIP adsorbent preparation. This study investigated the potential of modified bamboo biochar for CIP removal from aqueous solutions using batch adsorption experiments. The CIP adsorption process parameters such as initial CIP concentration, pH, contact time, and adsorbent dosage were optimized employing response surface methodology (CCD experimental design). Adsorption kinetics, isotherm, and thermodynamic studies were conducted to describe the removal mechanism and nature of CIP adsorption with modified bamboo biochar. Furthermore, adsorbent reuse and recycle test was conducted for five consecutive CIP adsorption-desorption cycles.

2. Materials and methods
2.1. Chemical and materials

The bamboo sawdust was collected from the local areas where bamboo is processed for furniture applications. All other chemicals ($FeCl_3.6H_2O$, KOH, HCl, NaOH, and NaCl) used in this study were purchased from Rankem chemical supplier, Ethiopia. The analytical standard for ciprofloxacin hydrochloride (CIP) with purity >99.7% was obtained from Cadila Pharmaceuticals Ltd in Addis Ababa, Ethiopia. All chemicals used in this study were analytical grade and used without further purification.

2.2. Adsorbent preparation

The collected bamboo sawdust was washed to remove any dirt bound to the biomass and dried overnight at 120ºC. Afterward, it was grounded to a particle size less than 850μm. Bamboo sawdust was chemically modified with ferric chloride and potassium hydroxide at the same time, employing a 5:1 w/w ratio of bamboo sawdust to $FeCl_3.6H_2O$ and a 1:5 w/v ratio of bamboo sawdust to KOH (1M). The chemical modification was carried out at 80ºC and 600 rpm for 2 hrs. The mixture was then dried at 60ºC in a vacuum oven for 24 hrs. The dried and chemically treated bamboo sawdust was grounded to a particle size of less than 450μm before being carbonized at 700ºC for 1 hr at a heating ramp rate of 10ºC/min in an oxygen-limited carbolite furnace. The carbonized bamboo (bamboo biochar) was then washed with ultrapure water until the filtrate pH became 7 and dried at 120ºC overnight to get modified bamboo biochar (MBC). The MBC was then grounded to a particle size less than 150 μm and stored in air-tight polyethylene bags for further use. Moreover, unmodified bamboo biochar (UBC), bamboo treated solely with ferric chloride (FMBC), and bamboo treated with only potassium hydroxide (KMBC) were also prepared via a similar synthesis route to investigate the effect of chemical modification and individual chemical modifications.

2.3. Adsorbent characterization

The structure and crystal phase of the modified (MBC) and unmodified bamboo biochar (UBC) were analyzed by conducting the x-ray diffraction analysis (XRD; Rigaku MiniFlex 600 Benchtop). In XRD analysis, Cu Kα radiation was applied to generate x-rays at 1.54441Å wavelength employing the following operational conditions: 40 kV and 15 mA, and angle scanning (2θ) ranging from 10° to 60°. Moreover, the presence of functional

groups was identified by Spectrum 65 PerkinElmer-FTIR in the range of 4000-400 cm^{-1} (resolution: 4cm^{-1}, no of scans: 16) using KBr pellets. In addition, the specific surface areas of the biochars were analyzed with nitrogen adsorption-desorption at 77 °K using SA-9600 Series Surface Area Analyzer (Horiba Instruments, Inc.). The samples were degassed at 100°C for 2h before analysis. The specific surface area was determined by the multi-point BET method in the N$_2$ relative pressure (P/P$_0$) range of 0.05–0.30.

2.3.1. Determination of pHpzc

The point of zero charge (pH$_{pzc}$) is one of the vital material characterization parameters that describes the net surface charge of adsorbents as a function of solution pH (Al et al., 2021; Khodadadi et al., 2019). The point of zero charge (pHpzc) of MBC was conducted according to the method used in previous studies (Khodadadi et al., 2019; Peña et al., 2012; Al et al., 2021). In this study, pH$_{pzc}$ was determined using eight Erlenmeyer flasks filled with 50 ml CIP solution (20 mg L^{-1}). Initially, the pH values of the solutions were adjusted to 2–11 using 0.1 M HCl and 0.1M NaOH. Following that, 0.1 g of the MBC was added to each flask and shaken at 200 rpm for 24h. The final pH values of the solutions were then measured. The variations between final and initial pH values were recorded (y-axis) and plotted against the initial pH values (x-axis). The initial pH value at which y-axis = 0 denotes the point of zero charge (pH$_{pzc}$) value.

2.4. Adsorption experiments

A preliminary batch adsorption study was undertaken to investigate the CIP removal efficiencies of UBC, MBC, FMBC, and KMBC. Based on the preliminary study, MBC showed superior performance on CIP removal and was chosen for further adsorption study. Batch adsorption experiments were conducted in a water bath shaker under controlled temperature and shaking speed. A stock solution of ciprofloxacin hydrochloride monohydrate (1 g L^{-1}) was prepared by dissolving 1000 mg of ciprofloxacin in one litre ultrapure water. The adsorption equilibrium time was determined at pH =7.0, CIP initial concentration of 20 mg L^{-1}, and adsorbent dosage of 0.5 g L^{-1} considering contact time of 10, 30, 50, 70, 90, 110, and 130 minutes. To obtain an optimal operational condition, adsorption process parameters such as CIP initial concentration (5–50 mg L^{-1}), pH = 2-12, contact time (5–60 min), and adsorbents dose (0.25–1.25 g L^{-1}) were studied. These parameter ranges were selected based on adsorption experiments (equilibrium study, point of zero charges, and preliminary test) as well as commonly reported operational conditions for CIP removal in the literature. The pH

of the CIP solution was adjusted using 0.1M HCl and 0.1M NaOH. All adsorption studies were carried out in a 100 ml conical flask using a water shaker bath at 200 rpm and 25ºC. The temperature was varied from 25 to 45ºC for the thermodynamic study. Before CIP analysis, the adsorption solution was centrifuged at 4000 rpm for 10 minutes and filtered through a 0.45μm syringe filter. Adsorption experiments of kinetics, isotherms, and thermodynamics were carried out in triplicate. Eqs.(1) and (2) were used to compute CIP removal efficiency and adsorption capacity, respectively (Falyouna et al., 2022).

$$\text{Re}\,moval \% = \frac{(C_o - C_t)}{C_o} * 100 \tag{1}$$

The adsorption capacity was obtained from the following equation:

$$q_t = \frac{(C_o - C_t)V}{M} \tag{2}$$

Where, C_0, C_t, V, and M are the initial CIP concentration (mg L^{-1}), ciprofloxacin concentration (mg L^{-1}) at a given time t (min), V is the volume of the solution (L), and mass of the adsorbent (g), respectively.

2.5. Ciprofloxacin analysis

Ciprofloxacin concentration was analyzed using a spectrophotometer (UV1610, China) at 274.8 nm. The calibration curve was plotted using seven standard ciprofloxacin solutions: 5, 10, 15, 20, 25, 30, and 35 mg L^{-1}, as well as a blank. The obtained standard calibration ($R^2 = 0.998$) curve is expressed in Eq. (3).

$$Y = 0.09117X + 0.02133 \tag{3}$$

where, Y is CIP concentration (mg L^{-1}), and X is the UV–vis spectrophotometer absorbance reading of the solution at 274.8 nm wavelength.

2.6. Adsorbent regeneration

Adsorbent reusability is one of the most important economic parameters of the adsorption systems in water and wastewater treatment applications (Abu Rumman et al., 2021). Therefore, in this study, the reusability of MBC was examined for five consecutive CIP adsorption-desorption cycles at an optimal operating conditions (pH = 7.5; CIP concentration = 20 mg L^{-1}; MBC dose = 0.5g L^{-1}, time = 120 min, shaking speed = 200 rpm

and temperature = 25ºC) obtained in previous steps. CIP desorption optimization experiments were conducted using 0.3M NaOH, 0.3M HCl, methanol, and 3% NaOH + methanol to get the best desorbing solution for the CIP. These solutions were employed in previous studies as eluents for CIP desorption from various adsorbents. The MBC reusability test was then conducted using the best desorbing solution. After each cycle, MBC was thoroughly washed with ultrapure water, filtered and dried up in an oven, and then reused in the next adsorption cycle. The adsorption efficiency of MBC after each cycle was calculated using Eq. (1).

2.7. Design of experiments using a central composite design

Central composite design (CCD) is one of the frameworks of response surface methodology (RSM) often employed to statistically analyze experimental data. Design expert software (Trial version: 11.0) was used to evaluate all parameters and experimental data. In this approach, responses are affected by various process variables. Main process variables such as pH, adsorbent dose, contact time, and CIP concentration were combined to give 30 experiments for CIP removal from an aqueous solution. An equilibrium time study and determination of the point of zero charges of MBC were conducted before developing the CCD experimental design. Thus, the selection of levels of pH and contact time was based on the data obtained from these studies and the review of previous studies. Levels of other parameters such as initial CIP concentration and adsorbent dose were based on the CIP adsorption preliminary study and commonly reported values in previous studies. Table 1 shows the independent variable ranges and their coded values. CIP has pKa values of 6.1and 8.7. In this regard, the pH values of low (5.25), central (7.5), and high (9.75) were selected to include the pH level less than 6.1, greater than 8.7, and 6.1 - 8.7. Low contact time (18.75 min) and high (46.25 min) were selected after conducting the equilibrium time study. Contact time values below the equilibrium time (70 min) were selected to analyze the effect of contact time on CIP adsorption. The relationship between the coded and real (un-coded) values is presented in Eq. (4) (Asghar et al., 2019a).

$$x_i = \frac{X_i - X_o}{\Delta X} \tag{4}$$

where x_i stands for the dimensionless coded value of the ith independent variable, X_i is the actual value of the independent variable, X_0 is the central point actual value, and Δx is the step change value of the variable.

Table 1. The independent variables and their levels in the CCD experimental design

Factors		Levels			Star points	
Actual	Coded	Low (-1)	Central (0)	High (+)	-α	+α
CIP initial concentration (mg L^{-1})	A	20	30	40	10	50
Adsorbent dosage (g L^{-1})	B	0.5	0.75	1.00	0.125	1.25
pH	C	5.25	7.5	9.75	3	12
Contact time (min)	D	18.75	30.00	46.25	5	60

In this regard, RSM was used to derive a quadratic polynomial model for expressing the effects of the independent variables on the response. The quadratic equation of the optimal model was given by Eq. (5) (Asghar et al., 2019a).

$$Y = \beta_o + \sum_{i=1}^{n=4} \beta_i X_i + \sum_{i=0}^{4} \sum_{j=1}^{4} \beta_{ij} X_i X_j + \sum_{i=1}^{4} \beta_{ii} X_j^{2} + \varepsilon \tag{5}$$

where Y is the model predicted response, β_0 is the coefficient of the model (constant), X_i (i =1 to 4) represents the independent variables, and βi, βii, and βij (i and j =1–4) indicate the linear, quadratic and second-order interaction coefficients, and ε is the corresponding error. Analysis of variance (ANOVA) was employed to statistically assess the potential of the developed polynomial model in predicting the experimental results.

2.8. Adsorption kinetic study

The time profile data of CIP adsorption onto the modified biochar were analyzed using four kinetic models commonly used in solid-liquid adsorption processes: the pseudo-first-order equation, the pseudo-second-order equation, Elovich, and intra–particle kinetic models as written in Eqs. (6-9), respectively (Soares et al., 2019). Adsorption kinetics was studied using the optimum parameters obtained in the RSM optimization step.

$$\ln(q_e - q_t) = \ln q_e - K_1 t \tag{6}$$

$$\frac{t}{q_t} = \frac{1}{K_2^{2} q_e^{2}} + \frac{t}{q_e} \tag{7}$$

$$q_t = \frac{1}{\beta}\ln(\alpha\beta) + \frac{1}{\beta}\ln t \tag{8}$$

$$q_t = K_{id}t^{\frac{1}{2}} + K_0 \tag{9}$$

where, q_e and q_t are the amounts of CIP (mg g^{-1}) adsorbed per unit mass of MBC at equilibrium and at a time t, respectively; K_1, K_2, and K_{id} are the pseudo-first-order (min^{-1}), pseudo-second-order (g mg^{-1} min^{-1}) and intraparticle mg (g min$^{0.5}$)$^{-1}$ rate constants, respectively. α (mg g^{-1} min^{-1}) indicates the initial adsorption rate, β (g mg^{-1}) represents the activation energy rate change with surface coverage, and K_o represents the thickness of the boundary layer.

2.9. Adsorption isotherm study

The adsorption performance of the CIP isotherm model is essential for investigating the interactions between CIP and biochar (MBC) during the adsorption process (Balarak et al., 2021). This study considered four isotherm models: Langmuir, Freundlich, Temkin and Dubinin–Radushkevich (D–R) to evaluate the equilibrium CIP adsorption isotherm data expressed in Eq. (10-13), respectively. The isotherm study was conducted using optimum operating conditions obtained from the CCD experimental design.

$$\frac{C_E}{q_e} = \frac{1}{q_m b} + \frac{C_e}{q_m} \tag{10}$$

$$\ln q_e = \ln K_F + \frac{\ln C_e}{n} \tag{11}$$

$$q_e = \beta\ln K_T + \beta\ln Ce \tag{12}$$

$$\ln qe = \ln qm - K\varepsilon^2 \tag{13}$$

where C_e is the equilibrium concentration of the CIP in solution (mg L^{-1}), q_e is the adsorption capacity at equilibrium (mg g^{-1}), b (L mg^{-1}) Langmuir constant, and q_m (mg g^{-1}) is the maximum adsorption capacity. The maximum monolayer adsorption capacity (q_m) and b were obtained from the slope and intercept of C_e versus C_e/q_e plot. K_F (mg g^{-1}) denotes the Freundlich isotherm constant. Freundlich intensity parameter (n) indicates existing adsorption driving forces and heterogeneity degree of the surface. The Temkin model constants, β and K_T (L mg^{-1}), are related to the heat of adsorption and maximum binding energy, respectively.

In the D-R model, K stands for adsorption energy constant, q_m represents the theoretical saturation capacity (mg g^{-1}), and ε is the Polanyi potential, calculated from Eq. (14). Based on the Langmuir equation, an essential parameter of adsorption (R_L) is expressed in Eq. (14).

$$R_L = \frac{1}{(1+bC_O)} \tag{14}$$

Where C_0 (mg L^{-1}) and b (L mg^{-1}) are initial CIP concentration and Langmuir constant, respectively. The calculated value of R_L can characterize the type of the isotherm and its nature: (i) irreversible isotherm (R_L=0); (ii) favorable isotherm ($0<R_L<1$); (iii) linear isotherm (R_L=1); unfavorable isotherm ($R_L>1$) (Li et al., 2018; Stylianou et al., 2021). The above D-R model can be evaluated using Eq. (15).

$$\varepsilon = RT \ln(1 + \frac{1}{Ce}) \tag{15}$$

The constant K is expressed by the slope of the plot of lnq_e vs. ε^2, and the adsorption capacity, q_m (mg g^{-1}), can be obtained from the intercept.

2.8.5. CIP adsorption thermodynamic study

The thermodynamic study was conducted using 25, 35, and 45ºC at a shaking speed of 200 rpm. Optimum CIP adsorption conditions obtained in the CCD design were employed to conduct the thermodynamic study. There are three essential parameters for thermodynamic study, namely, Gibbs free energy change (ΔG^o), enthalpy change (ΔG^o), and entropy change (ΔG^o). Gibbs free energy change (ΔG^o) can be evaluated by applying Van't Hoff equation.

$$\Delta G° = -RT \ln K_o \tag{16}$$

where, T, R, and K_o are absolute temperature (K), universal gas constant (8.314 J K^{-1} mol^{-1}), and thermodynamic constant (dimensionless), respectively. The third principle in thermodynamics emphasizes the relationship between ΔG^o and the other two parameters in Eq. (17).

$$\Delta G° = \Delta H° - T\Delta S° \tag{17}$$

where, ΔG^0, ΔH^0, and ΔS^0 are Gibbs free energy change (J mol^{-1}), enthalpy change (J mol^{-1}), and entropy change (J mol^{-1} K^{-1}). Combining Eq. (16) and (17) will generate a new formula for Van't Hoff equation expressed in Eq. (18). Based on Eq. (18), ΔG^o and ΔS_0 of the reaction can be determined from the slope and the intercept of the plot of lnK$_o$ (Y-axis) versus T^{-1} (X-axis).

$$\ln Ko = -\frac{-\Delta H^0}{RT} + \frac{\Delta S^0}{R} \qquad (18)$$

3. Results and discussion

3.1. Characterization of biochar

3.1.1. FTIR analysis

The FTIR spectra of unmodified biochar (UMC), modified biochar (MBC), modified biochar after CIP adsorption (MBC-CIP) and CIP are presented in Fig. 1. In MBC, new peaks appeared at 3543 – 3456 cm^{-1} (broad peak), 2918 – 2835cm^{-1}, 2250 – 2000, and 1052 cm^{-1}, which were assigned to the stretching vibrations of –OH (hydroxyl or carboxyl groups (Peng et al., 2018), C-H (asymmetrically and symmetrically stretching vibrations of aliphatic), C≡O (alkyne) and C-O (carboxylic acid and esters), respectively. The dehydration of biochar (chemically treated) sample during the carbonation process resulted in the O-H vibration stretching of water molecules (Al et al., 2021). Additionally, the new peak emerged in MBC at 540 cm^{-1} shows Fe-O-Fe stretching vibration, indicating that iron oxide was successfully supported on the biochar surface (Ma et al., 2022; Al et al., 2021). Thus, the FTIR spectra result showed that the surface of MBC contained rich oxygen-containing groups and aromatic structures, which provided favorable conditions for CIP adsorption.

After CIP adsorption onto MBC (CIP-MBC), as shown in Fig 1, the peaks observed in MBC at 3500, 2872, and 1052 cm^{-1} were shifted to 3407, 2917, and 1018 cm^{-1}, respectively. On the other hand, the peaks observed at 2188 and 540 disappeared after adsorption. Moreover, the new narrow peak (2920 cm^{-1}) that appeared on MBC-CIP is similar to the peak observed in CIP (2920 cm^{-1}). The intensity of the peak observed in MBC after adsorption (MBC – CIP) at 3400 cm^{-1} is similar to the intensity of the peak at 3500 in CIP. Hence, it is evident that the –OH, C-H, C-O, C≡O, and Fe-O groups observed on MBC were involved in the CIP adsorption process. The presence of several functional groups on

the surface of MBC played an important role in CIP removal from aqueous solution via electrostatic interactions, complexation reaction, π-π EDA interactions, and hydrogen bonding (Rajapaksha et al., 2019).
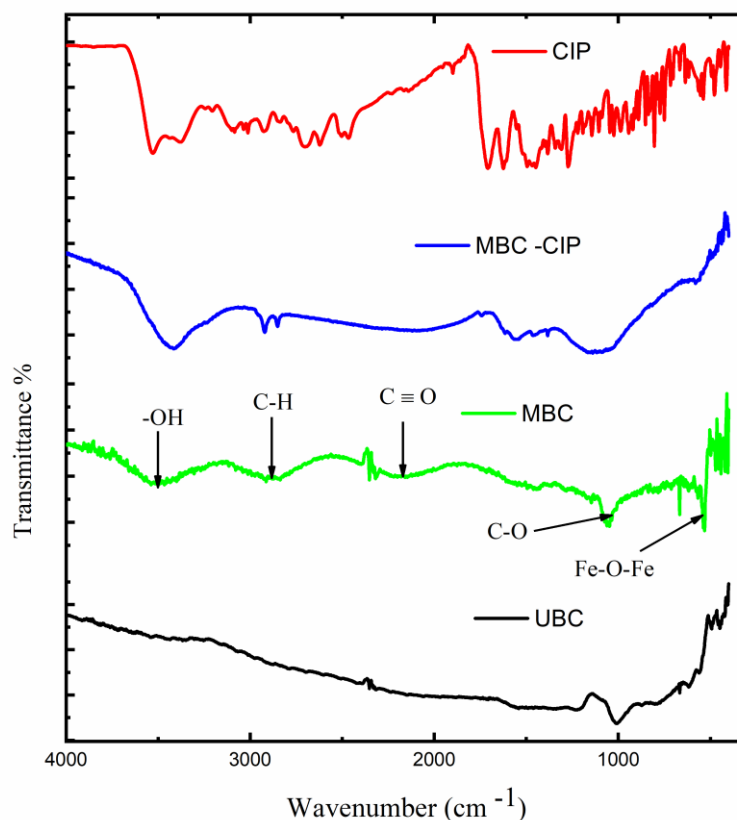

Figure 1. FTIR spectra of unmodified (UBC), modified biochar (MBC), modified biochar after adsorption (MBC - CIP), and ciprofloxacin (CIP)

3.1.2. BET surface area

The BET surface area of MBC (1158.050 $m^2\ g^{-1}$) was remarkably higher than that of UBC (565.095 $m^2\ g^{-1}$). This result indicated that simultaneous activation of bamboo sawdust with ferric chloride and potassium hydroxide enhanced the surface area of the biochar significantly. The increase in surface area may be attributed to the formation of new pores and the opening of initially inaccessible pores during the chemical activation process, which would help develop a more porous structure (Peng et al., 2018). The surface area is an important parameter that plays a significant role in physical adsorption. The higher surface area of the material leads to higher adsorption of the pollutant due to the availability of many

adsorption sites for more organic pollutant removal (Peng et al., 2018). Accordingly, MBC is expected to have higher removal of CIP molecules from aqueous solutions than the UBC.

3.1.3. XRD

The X-ray powder diffraction (XRD) (XRD; Rigaku MiniFlex 600 Benchtop) was conducted to investigate the crystalline compositions of the bamboo biochars. The XRD analysis result is shown in Fig. 2. The peaks at 30.1, 35.6, 43.2, and 57.2 are assigned to magnetite (Kong et al., 2017), whereas the peak observed in MBC at 33.2 is assigned to hematite. The emergence of these peaks on the surface of MBC confirmed the presence of Fe-O in the structure of the modified biochar adsorbent. Al et al., (2021) detected a peak at a similar angular degree for Fe_3O_4 cubic crystals on an adsorbent prepared from powdered activated carbon magnetized by iron (III) oxide magnetic nanoparticles.
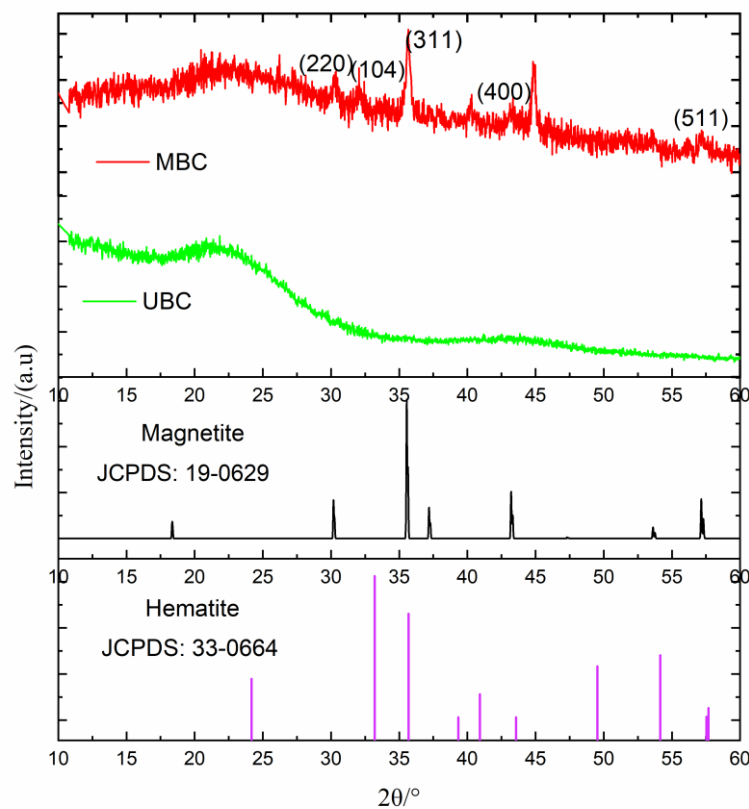

Figure 2. XRD patterns of raw and modified biochars

Iron (Fe) was believed to be present on the surface of modified biochar (MBC) as indicated by characteristic peaks of magnetite and hematite (He et al., 2018; Mian et al., 2018; Gong et al., 2016). The XRD result revealed that Fe was successfully loaded onto the MBC, which is

consistent with the findings of the FTIR analysis. Therefore, the chemical modification of the biochar has desirable structural changes on the biochar, as evidenced by the XRD plot.

3.1.4. Point of zero charge (pH_{pzc})

Determining pH_{pzc} is essential for the adsorption process study as the adsorption mechanism strongly depends on the solution pH. The point of zero charge of MBC is about 6.5, as shown in Fig S1. Based on the pH_{pzc} result, the surface of MBC is positively charged when pH is below 6.5 and negatively charged when pH is above 6.5. At pH below 6.0, ciprofloxacin is mainly present in its cationic form (Peng et al., 2018), and the surface of the MBC is positively charged. Hence, the adsorbent and ciprofloxacin molecules repel each other, and thus CIP removal efficiency decreased. Increasing pH above 6.1 changes the CIP molecule from cationic to zwitterionic leading to a gradual increase in CIP adsorption (Atugoda et al., 2021). Due to the strong electrostatic interaction between MBC and CIP zwitterion (pH 6.0-8.7), maximum adsorption was obtained.

In contrast, at pH higher than 8.7, the adsorption process efficiency decreased as the repulsive force increased between the negatively charged MBC surface and anionic CIP molecules (Asghar et al., 2019b). Similar results were obtained by Asghar et al. (2019b) in removing ciprofloxacin from water using γ-Al_2O_3 nanoparticles. Consistently, Ji et al. (2021) reported similar results with a pH range (6–8) as an optimal condition for titanate nanotubes to remove CIP molecules.

3.2. Adsorption of CIP onto MBC adsorbent

In this work, different bamboo-based adsorbents: unmodified bamboo biochar (UBC), bamboo biochar modified with ferric chloride (FBC), bamboo biochar modified with potassium hydroxide (KMBC), and bamboo biochar modified with both ferric chloride and potassium hydroxide (MBC) were prepared. The CIP removal efficiencies and adsorption capacities of the as-synthesized bamboo-based adsorbents are shown in Table 2. MBC was prepared chemically by modifying the bamboo sawdust with ferric chloride and potassium hydroxide at the same time as depicted in section 2.2. As shown in Table 2, the UBC, FMBC, KMBC, and MBC gave 45.01, 67.38, 79.45, and 95.67% CIP removal, respectively. This experiment was conducted at CIP initial concentration (25 mg L^{-1}), adsorbent dose (0.5 g L^{-1}), contact time (46.25 min), and pH (7.0). The result indicated that modification of the bamboo by KOH, $FeCl_3$, or KOH/$FeCl_3$ has resulted in increased CIP removal. The high adsorption

capacity can be ascribed to the high surface area of the adsorbent (1158.05 m^2/g) and the strong interaction of CIP molecules with MBC surface functional groups.

MBC has remarkably superior adsorption capacity (78.43 mg g^{-1}) than all other bamboo-based adsorbents (UBC, FMBC, and KMBC). This may be attributed to the collaborative effect of both KOH and $FeCl_3$ activation. Fe-O group was detected on the surface of the MBC as confirmed by XRD and FTIR spectra analysis. The high adsorption performance observed for KOH/$FeCl_3$ modified adsorbent is may be due to the formation of Fe-O sorption sites (Chen et al., 2011; Zhao et al., 2018; Chen et al., 2019; Reguyal et al., 2016) in addition to the formation of -OH, C-H, C-O, C≡O functional groups. Iron functional groups may form a complex reaction with CIP zwitterions increasing CIP removal from aqueous solution. Hence, MBC (bamboo biochar with combined modification) was selected and used as the best adsorbent throughout this study. The adsorbent has magnetic properties because of iron which may help during the separation of the adsorbent.

Table 2. Adsorbent screening test for CIP removal

Adsorbent	Short name	% CIP removal	Decision
Unmodified bamboo biochar	UBC	45.01	Not selected
Ferric chloride modified bamboo biochar	FMBC	67.38	Not selected
Potassium hydroxide modified bamboo biochar	KMBC	79.45	Not selected
Ferric chloride + potassium hydroxide modified bamboo biochar	MBC	95.67	selected

*Experimental condition: CIP initial concentration: 25 mg L^{-1}, adsorbent dose: 0.5 g L^{-1}, time 46.25 min and pH: 7.0

3.2.1. Model fitting and analysis of variance (ANOVA) using CCD

The central composite design (CCD) was used to optimize the CIP adsorption process parameters. The CCD experimental design of CIP adsorption data is presented in Table S1. The second-order polynomial model fitted the experimental data of CIP adsorption onto MBC ($R^2 = 0.9861$). The suggested quadratic model's R^2 and adjusted R^2 were 0.9904 and 0.9861, respectively. ANOVA was used to assess the validity and adequacy of the model and determine the effect of main factors and possible interaction factors. ANOVA indicated that the suggested polynomial model was statistically significant. The result of the ANOVA analysis is presented in Table 3. As shown in Table 3, the F- and p-values of the model were

229.46 and < 0.0001, respectively. There is only a 0.01% chance that an F-value this large could occur due to noise. A, B, C, D, AB, BD, CD, B², and C² are significant model terms from the ANOVA table. Hence, all the independent variables (initial CIP concentration, pH, contact time, and adsorbent dosage) significantly affected the CIP removal. Both Yousefi et al. and Asghar et al. reported similar findings for the CIP removal using magnetization of functionalized multi-walled carbon nanotubes and γ-Al_2O_3 nanoparticles as an adsorbent, respectively (Yousefi et al., 2021; Asghar et al., 2019a). In their studies, adsorption parameters including initial CIP concentration, pH, contact duration, and adsorbent dose, were significant in CIP removal from an aqueous solution.

Model terms with p-values less than 0.05 are significant, and terms with p-values higher than 0.05 are not significant. Relative to pure error, the Lack of Fit is not significant, as indicated by the Lack of Fit F-value of 1.74. There is a 28.06% chance that a Lack of Fit F-value this large could occur due to noise. As a result, a lack of fit that is not significant is desired since we want the model to fit the CIP experimental data well. Adeq precision measures the signal-to-noise ratio and a value greater than 4 is desirable. In this design, the ratio of 56.593 indicates an adequate signal. This model can be used to navigate the design space successfully.

Table 1. ANOVA results of the CIP adsorption onto MBC

Source	Sum of Squares	df	Mean Square	F-value	p-value	
Model	4671.16	9	519.02	229.46	< 0.0001	significant
A-Initial CIP Con	787.42	1	787.42	348.12	< 0.0001	
B-Adsorbent dose	2224.34	1	2224.34	983.38	< 0.0001	
C-pH	144.01	1	144.01	63.67	< 0.0001	
D-Contact time	691.76	1	691.76	305.83	< 0.0001	
AB	326.80	1	326.80	144.48	< 0.0001	
BD	129.79	1	129.79	57.38	< 0.0001	
CD	138.47	1	138.47	61.22	< 0.0001	
B²	150.60	1	150.60	66.58	< 0.0001	
C²	102.79	1	102.79	45.45	< 0.0001	
Residual	45.24	20	2.26			
Lack of Fit	37.98	15	2.53	1.74	0.2806	not significant
Pure Error	7.26	5	1.45			
Cor Total	4716.40	29				

df: degree of freedom

Based on the CCD statistical analysis, the final predicted model equation in terms of coded factors is expressed in Eq. (19) with significant factors (main and interaction). In Eq. (19), A, B, C, and D are the coded values of initial ciprofloxacin concentration, adsorbent dose, pH, and contact time, respectively. Whereas, AB, BD, and CD are the significant interaction parameters.

$$CIP\,\mathrm{Re}\,moval = 89.49 - 5.73A + 9.63B - 2.45C + 5.37D + 4.52AB - 2.85BD + 2.94CD$$
$$- 2.30B^2 - 1.90C^2 \tag{19}$$

The influence of each factor on the removal of CIP can be seen from their coefficients in Eq. (19). The coefficients of each factor are -5.98, 9.38, -2.70, and 5.12, respectively, confirming that A and C have a negative effect, whereas B and D have a positive effect on the CIP removal. The results displayed in Table 3 indicated that the influence of each parameter on the CIP removal followed the order: B > A > D > C, which is in agreement with the results described in Eq. (19). Notably, the adsorbent dose and the initial concentration of CIP had the most significant effect on the CIP removal process. Also, the final equation in terms of the actual factors for CIP adsorption onto MBC is presented in Eq. (20).

$$CIP\,\mathrm{Re}\,moval = 75.058 - 1.92*initialCIP + 1328.55*adsorbentdose + 1.45*pH + 0.29*$$
$$contact\,time + 36.15*initilalCIP*adsorbentdose - 16.57*adsorbentdose*contact\,time +$$
$$0.09*pH*contact\,time - 14726.5*adsorbentdose^2 - 0.37*pH^2 \tag{20}$$

According to the model fit statistics, the regression parameters such as the coefficient of determination (R^2), adjusted coefficient of determination, and predicted determination coefficients are 0.9876, 0.9820, and 0.9670, respectively. Thus, the model represents 98% of the variation in the CIP removal response. The values of model regression parameters indicate proper fitness of the model as shown in Table 2. Using the CCD experimental design, Asghar and his co-workers reported similar model fit statistics values ($R^2 = 0.96$) for the CIP adsorption (Asghar et al.,2019b).

Diagnostic plots such as externally studentized residuals against predicted, predicted against actual, and the normal probability against externally studentized residuals were analyzed to assess the model's adequacy. These results are presented in Fig S2 (a-c). The normal probability against externally studentized residual plot shown in Fig S2 (a) indicated that all the points are close to the straight line, showing that the error was normally distributed. From the plot of predicted against actual shown in Fig S2 (b), it can be seen that

the predicted values are well correlated with the actual (experimental) values, and the model predicted data were not significantly different from the experimental results. The highest residual (difference between actual and predicted) is 2.93 for the CIP removal of 88.35%. In a plot of externally studentized residuals against predicted shown in Fig S2 (c), the residuals were randomly distributed between +3.00 and −3.00, indicating that the CCD model successfully established the relationship between the independent variable and the CIP removal (Peng et al., 2021). Overall, the diagnostic plot results agree with the coefficient of determination values of the model. Thus, the quadratic model suggested by CCD experimental design described the experimental CIP adsorption data adequately.

3.2.2. Effect of individual process variables

The effect of the adsorption process variables such as pH, initial CIP concentration, adsorbent dose, and contact time on CIP removal was investigated. Fig S3 (a-d) displays the one factor plots for each main factor. These include initial CIP concentration, adsorbent dose, pH, and contact time.

Effect of CIP initial concentration

The effect of initial CIP concentration on the adsorption efficiency was investigated. Fig S3(a) depicted that increasing the CIP initial concentration from 10 to 40 mg L^{-1} decreased the CIP removal efficiency from 100 to 75.52% at pH (7.5), adsorbent dose (0.5 g L^{-1}), and contact time (46.25 min). In line with this result, Yousefi et al. reported that increasing the CIP concentration from 30 to 100 mg L^{-1} decreased CIP removal efficiency from 83% to 59% (Yousefi et al., 2021). On the other hand, Wang et al. investigated the effect of the initial CIP concentration (10–200 mg L^{-1}) at pH (6) and adsorbent dosage (135 mg L^{-1}) on the adsorption capacity. In their study, the adsorption capacity of the adsorbent for cationic CIP increased very quickly for CIP initial concentration of less than 50 mg L^{-1} and then decreased with the increase of CIP initial concentration above 50 mg L^{-1} (Wang et al., 2018). Hence, an increase in CIP initial concentration decreased the removal efficiency. This may be attributed to the lack of available sites on the adsorbent for the uptake of high CIP concentration (El-bendary et al., 2021). In this study, unlike the case for CIP percentage removal, the CIP adsorption capacity increased from 20 mg g^{-1} to 60 mg g^{-1} by increasing the initial CIP concentration from 10 to 40 mg L^{-1}. This is due to the reduction of the resistance to CIP uptake from the aqueous solution. Moreover, the higher initial CIP concentration

provides a driving force to overcome the mass transfer resistance of the CIP between the solid and aqueous phases (El-bendary et al., 2021).

Effect of adsorbent dose

The adsorbent dose has a significant effect on the CIP removal from an aqueous solution. As depicted in Fig S3(b), using an adsorbent dose of 0.25g L^{-1} at pH 7.5, 30 mg L^{-1} initial CIP concentration, and 46.25 min contact time resulted in 96.02 % CIP removal, whereas using an adsorbent dose of 1.0 g L^{-1} at similar adsorption conditions almost completely removed CIP from the solution. A similar adsorption trend was observed by (Gulen and Demircivi, 2020) in the adsorption of CIP from water using a 2: 1 dioctahedral clay structure with the increase of CIP adsorption from 1.8% (0.034 g L^{-1}) to 99.2% (2 g L^{-1}). Moreover, Shang et al. reported a significant increase in the CIP removal efficiency from 36 to 100%, for an increase in adsorbent (herbal residue biochar) dosage from 0.025 to 0.5 g L^{-1} (Shang et al. 2016). The increase in the percentage of CIP removal with an increase in adsorbent dose is because of the increase of available active sites, which enhanced the CIP uptake (Khoshnamvand et al., 2017; Asghar et al., 2019b).

Effect of pH

The pH of the solution is an important parameter of adsorption processes because it affects the surface nature of the adsorbent and adsorbate-adsorbent interactions (Asghar et al., 2019b). At pH less than pKa_1 (6.1), the amine group in piperazine moiety receives a proton, and CIP^+ appears. However, for pH above pKa_2 (8.7), CIP occurs in anionic form (CIP^-) due to amine group deprotonation. At pH between pKa_1 and pKa_2 of CIP, the CIP molecule exists in zwitterionic form due to the charge balance of the amine and carboxylic groups (Zhang et al., 2017; Yousefi et al., 2021). Fig S3(c) depicted that the CIP removal efficiency of MBC increased by increasing the pH of the solution from 5.25 to 7.5 and then decreased with any further increase in pH. Hence, increasing pH from 5.25 to 7.5 at fixed initial CIP concentration (20 mg L^{-1}), adsorbent dose (0.5g L^{-1}), and contact time (46.25 min) increased the CIP removal from 93.62% to 96.02%. Further elevation of pH to 9.75 reduced the CIP removal to 94.61%. Thus, the optimal pH for CIP adsorption onto the MBC is 7.5. This pH level is very important since ciprofloxacin forms zwitterion and that led to the strong electrostatic attraction between CIP and negatively charged MBC. Hence, maximum adsorption was obtained at this pH level. Dehghan et al. (2019) observed a similar adsorption trend for the CIP using a metal organic framework (MOF). They reported that an increase in

pH from 3 to 7.5 increased the adsorption of CIP onto MOF. However, at pH values above 7.5, CIP adsorption decreased. The reason for this adsorption behavior can be attributed to protonation–deprotonation reactions in groups of CIP molecules (Dehghan et al., 2019).

Effect of contact time

Contact time is one of the significant factors in the adsorption of the CIP onto the MBC in this work. As shown in Fig S3 (d), adsorption at an adsorbent dose (0.5 g L^{-1}), pH (7.5), CIP initial concentration (20 mg L^{-1}), and the contact time (18.75 min) resulted in 79.58% of CIP removal. However, CIP removal efficiency increased to 96.02 % under similar adsorption conditions when the contact time increased to 46.25 min. Moreover, Fig S4 showed that the adsorption rate was rapid in the first 30 minutes and moderate in 30-70 minutes. This may be attributed to the availability of abundant free active sites on MBC at the initial adsorption stage for CIP sorption. The rate became very slow after 70 minutes, and no appreciable CIP removal was achieved. Hence, equilibrium was reached at about 70 min. The number of available active sites decreases with time, and eventually, the adsorbent becomes saturated (El-bendary et al., 2021). For CIP adsorption process optimization, adsorption experiments were conducted using the contact time range (less than 60 min), which is intentionally taken to fully investigate the effect of contact time and its interaction effects. Increasing the contact time allowed CIP molecules to reach the active sites of the adsorbent up to equilibrium time. Beyond the equilibrium time, no significant uptake of CIP took place as depicted in Fig S4.

3.2.3. Interaction effects of process variables

Response surface methodology is a powerful tool with important features for evaluating the interactive effect of variables. In this study, 3D surface plots (Fig 3 (a-c)) were employed to study the interaction effects on the CIP removal. The significant interaction effects include initial CIP concentration-adsorbent dose, adsorbent dose-contact time, and pH-contact time.

CIP initial concentration and adsorbent dose interaction effect

The interaction effect of CIP initial concentration and the adsorbent dose was shown in Fig 3 (a). The interaction effect of CIP initial concentration and the adsorbent dose was positively significant. From the 3D plot, it was observed that the CIP removal was highest at the initial CIP concentration range of 20-25mg L^{-1} and adsorbent dose range of 0.75–1.0 g L^{-}

[1]. The enhanced removal of CIP at the higher MBC dose was due to higher active sites for CIP adsorption (Bhattacharya et al., 2021).

Adsorbent dose and contact time interaction effect

The interaction effect of MBC dose and the contact time on CIP removal is displayed using a 3D plot in Fig 3 (b). CIP removal was highest at the MBC dose of 0.75-1.0g L^{-1} and at the reaction time of 40-46 min. This study revealed that CIP removal increased with an increase in contact time and adsorbent dose. This is may be attributed to the availability of more active sites with adsorbent dose increment and enough contact time for MBC and CIP molecules to interact with each other (Bhattacharya et al., 2021).

pH and contact time interaction effect

The interaction effect of pH and contact time on CIP removal is shown in Fig 3 (c). The percentage of CIP removal increased with an increase in contact time. A kinetics study showed that the adsorption rate was rapid in the first 30 minutes and became slow after 30 minutes. The CIP adsorption is strongly dependent on the pH of the solution. CIP exists in zwitterion form at pH between 6.1 and 8.7, and the electrostatic interaction between CIP and MBC is strong. The point of zero charge of MBC was 6.5, and for pH less than 6.1 and beyond 8.7, the repulsive forces became dominant, and less CIP removal was achieved. Thus, this pH range is an optimum pH level for the highest CIP removal. Fig 3 (c) depicted that when pH decreased from 9.75 to 5.25 with an increase in contact time from 18.75 to 46.25 min, the CIP removal increased from 71.88 to 93.62%. In contrast, an increase in pH and a decrease in contact time decreased CIP removal. The reverse of this condition decreased the CIP removal. This showed that contact time had a superior influence on CIP removal than pH for interaction effects. However, for an increase in pH and contact time from 5.25 and 18.75min to 9.75 and 46.25min, CIP removal increased from 83.07 to 94.61%, respectively. Maximum CIP removal (96.02) was obtained at pH (7.5) and contact time (46.25 min) using MBC adsorbent.
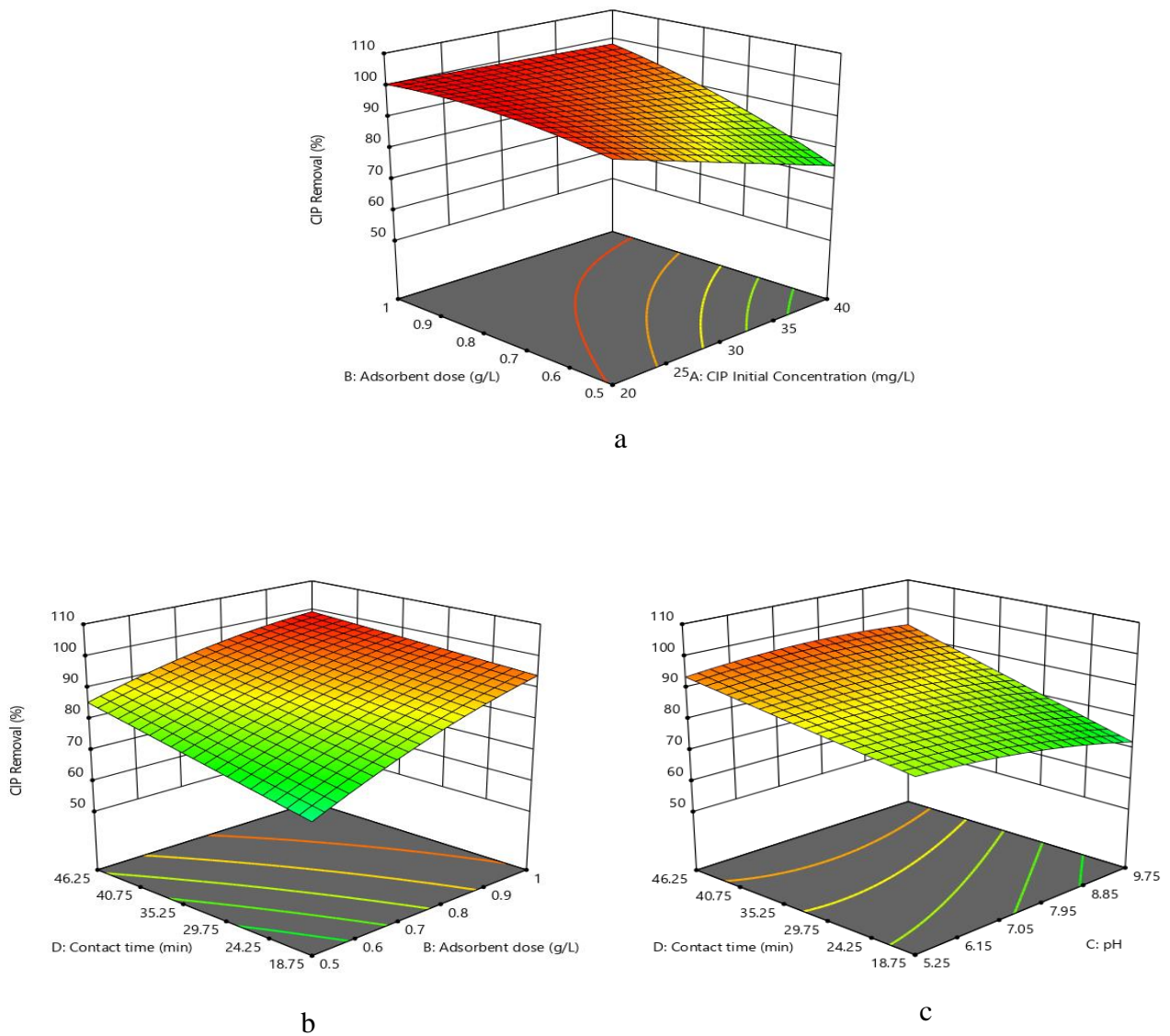
Figure 3. Interaction effects (a) adsorbent dose versus CIP initial concentration (b) contact time versus adsorbent dose (c) contact time versus pH

3.2.4. Process optimization

The optimization approach followed in CCD design to obtain the best operating conditions was by minimizing the adsorbent dosage, taking the initial CIP concentration in the range, pH in the range, and contact time in the range, and by maximizing CIP removal. Based on this criterion, the optimal condition that gave maximum CIP removal efficiency (96.02%) using the MBC adsorbent was pH (7.5), adsorbent (0.5 g L^{-1}), contact time (46.257 min), and initial CIP concentration (20 mg L^{-1}) with a good desirability value of 0.971. Adsorption tests were conducted at these optimum conditions to confirm the model's

credibility. Accordingly, CIP removal values of 95.68, 96.42, and 96.24 were obtained, and the mean value of these results is 96.11%. Thus, the model predicted CIP removal (96%) is close to the experimental value obtained (96.11%), showing that the model is valid.

3.3. Adsorption kinetics

The kinetic study determines the effect of contact time on CIP adsorption onto MBC. The results of CIP adsorption kinetics parameters are described in Table 4. The kinetic models are presented in Fig 4 (a-d). Initially, the sorption process was vigorous due to abundant free actives sites on the biochar surface where CIP molecules can be sorbed quickly. With time, the unoccupied active sites reduced significantly, declining the solution and solid adsorption rate to attain a steady state (Atugoda et al., 2021).

As shown in Table 4, the pseudo-second-order model has the highest coefficient of determination (R^2 = 0.994) compared to other kinetic models. In addition, q_e (calculated) using a pseudo-second-order kinetic model is very close to the experimental q_e. Hence, the pseudo-second-order model provided the best fit for the CIP experimental data as shown in Fig 4 (b), suggesting that the rate of ciprofloxacin adsorption onto the MBC followed the pseudo-second-order model. Overall, these results suggest that chemisorption controlled the rate of CIP adsorption (Soares et al., 2019; Balarak et al., 2021), which involves covalent bonding through sharing electrons between MBC and CIP molecule (Atugoda et al., 2021). More specifically, the π-π interaction, complexation reaction, and hydrogen bonding may have played a role in the chemisorption process. Similar findings have been reported in the literature (Wang et al., 2015).

The intraparticle diffusion model was employed to investigate the rate-controlling step (Ngeno et al., 2016). As the K_o increases, the contribution of the surface sorption in the rate-controlling step increases. The linear fit plot of qt versus $t^{0.5}$ is displayed in Fig 4 (d). The simple plot of qt versus $t^{0.5}$ for the intraparticle model presented in Fig S5 showed multi-linear behavior. This suggests that the adsorption process possessed multiple steps. Solute adsorption by porous adsorbents consists of three consecutive steps (Balarak et al.,2021). The first step represents the improvisational or external adsorption process. The second step is the intraparticle diffusion phase having gradual adsorption that occurs when intraparticle diffusion is rate-limiting. The last step is regarded as a final equilibrium phase in which the intraparticle diffusion starts to slow down due to a significantly lower adsorbate concentration. The intraparticle diffusion is the rate-limiting step when the regression line

passes through the origin. In contrast, when the regression line does not pass through the origin, other mechanisms can control the adsorption process in addition to intraparticle diffusion.

The plots showed a multi-linear trend, indicating that there were three steps during the CIP adsorption process, as shown in Fig. S5. The first stage occurred from 0 to 30 $min^{0.5}$ and represented boundary layer mass transfer (Balarak and Mckay, 2021). The second linear segment included the adsorption period from 30–80 $min^{0.5}$ and which represents the intraparticle diffusion process. The third stage took place between 80 and 120 $min^{0.5}$ and adsorption of CIP molecules occurred on the interior surface of the MBC. The last stage showed quite low slope due to the decrease in CIP concentrations (Zhang et al., 2017) and available active sites (Balarak et al., 2021) suggesting that the adsorption equilibrium was reached. In the first step, the adsorption rate was rapid, indicating a fast removal of CIP, while in the subsequent steps, the adsorption process decreased due to the decrease in CIP concentrations and available active sites (Balarak et al., 2021). Also, the low linear dependency of CIP adsorption on $t^{0.5}$ indicated that the CIP adsorption dynamics seemed to be less influenced by the intraparticle diffusion mechanism (Ngeno et al., 2016). On the other hand, the high K_o parameter value showed that the effect of the boundary layer was also responsible for the CIP adsorption onto MBC. Hence, it was noted that the adsorption of CIP onto MBC was enhanced due to the high surface area of the MBC and by the involvement of various functional groups on the surface of biochar (Atugoda et al., 2021). Overall, the adsorption rate of CIP onto MBC was jointly controlled by liquid film diffusion, surface adsorption, and intraparticle diffusion (Huang et al., 2018).

Table 4. Kinetic models and values of their parameters

Pseudo-first order model				Pseudo – second order			
K_1 (min-1)	$q_{e, cal}$ (mg g^{-1})	$q_{e,exp}$ (mg g^{-1})	R^2	K_2 (g mg^{-1} min^{-1})	$q_{e, cal}$ (mg g^{-1})	$q_{e, exp}$ (mg g^{-1})	R^2
0.05072	39.60	5.029	0.813	0.011	39.60	40.387	0.994
Intraparticle model				Elovich			
K_{id} (mg g^{-1} $min^{-1/2}$)	K_o	R^2		α (mg g^{-1} min^{-1})	B (g mg-1)	R^2	
3.27283	11.894	0.640		0.121	15.904	0.859	

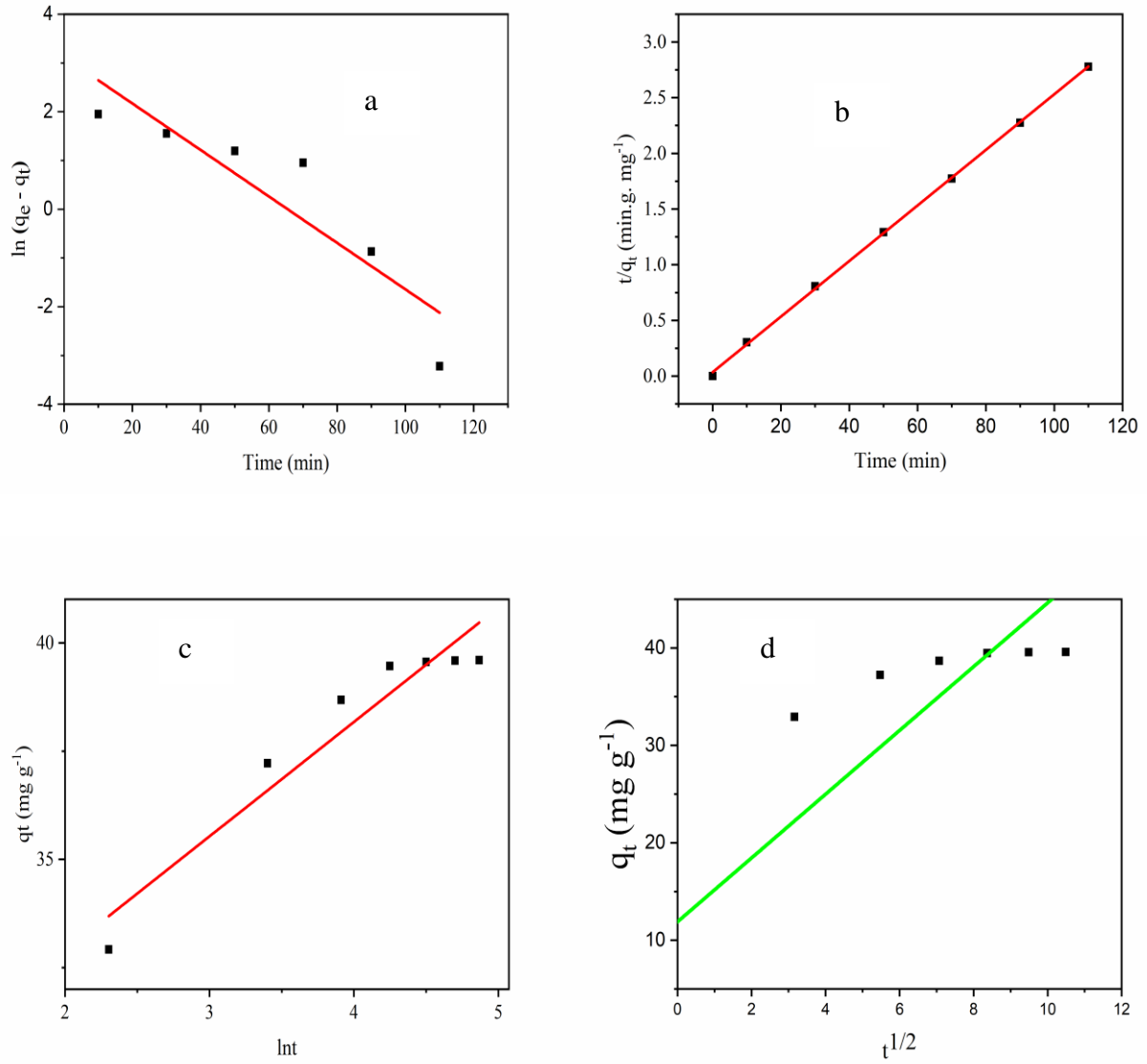Note: $q_{e, cal}$: calculated adsorbent capacity, $q_{e, exp}$: experimental adsorbent capacity

Figure **4**. Kinetic models of CIP adsorption onto MBC (a) Pseudo-first-order, (b) Pseudo-second-order, (c) Elovich and (d) intraparticle models

3.4. Adsorption isotherms

The isotherm models are crucial for adsorption processes because the isotherm models can provide maximum sorption capacity and the expected interactions between adsorbent and adsorbate (Balarak et al., 2021). This study considered four isotherm models to interpret and describe CIP adsorption data, including Langmuir, Freundlich, Temkin, and Dubinin- Radushkevich (DR). Adsorption isotherm parameters were evaluated and presented in Table 5. Also, the plots of CIP adsorption isotherm are presented in Fig 5 (a-d). An increase in initial concentration increased CIP adsorption capacity because the binding sites could easily come into contact with the adsorbate. After the saturation of the active sites at a

particular concentration, the adsorption remains unaffected with initial concentrations (Atugoda et al., 2021).

From the Langmuir isotherm, the calculated value of R_L using Eq.(13) can characterize the type of the isotherm and its nature: (i) irreversible isotherm ($R_L=0$); (ii) favorable isotherm ($0 <R_L<1$); (iii) linear isotherm ($R_L=1$); unfavorable isotherm ($R_L>1$) (Li et al., 2018; Stylianou et al., 2021). In this study, R_L was 0.0264, which depicted that the CIP adsorption process by MBC was favorable. The results of regression coefficients indicated that the Langmuir ($R^2 = 0.99$) model fits the adsorption process well, as shown in Fig 4 (a). Langmuir and Freundlich isotherm models fitted the CIP adsorption data reasonably, as described in Fig 4 (a) and (b), respectively. Conformity to these models showed that the MBC surface nature was heterogeneous, and this result is consistent with the intraparticle kinetic study that hypothesized the multi-mechanistic nature of CIP adsorption onto MBC (Sharifpour et al., 2020).

In this study, the MBC surface heterogeneity was confirmed by the Freundlich constant, $1/n$, which was 0.11 and lay between 0 and 1 for heterogeneous surfaces. In this model, if the value of n is higher than 10, an irreversible isotherm is obtained. Values of n greater than unity indicate preferential adsorption, and less than unity indicates poor adsorption. In the present study, the value of n is greater than unity, as indicated in Table 5. Hence, the adsorption of CIP onto MBC was favorable. It can be concluded that the adsorption process was monolayer adsorption on a heterogeneous surface which is in agreement with the previous work by (Li et al., 2018). The functional groups of the modified biochar (MBC) responsible for the CIP adsorption include the OH, C-H, C-O, C≡O, and Fe–O –Fe. These functional groups on the biochar provided a heterogeneous surface. According to the experimental findings, CIP adsorption onto these functional groups of the MBC would be in a monolayer fashion.

Table 2. Isotherm models and values of their parameters

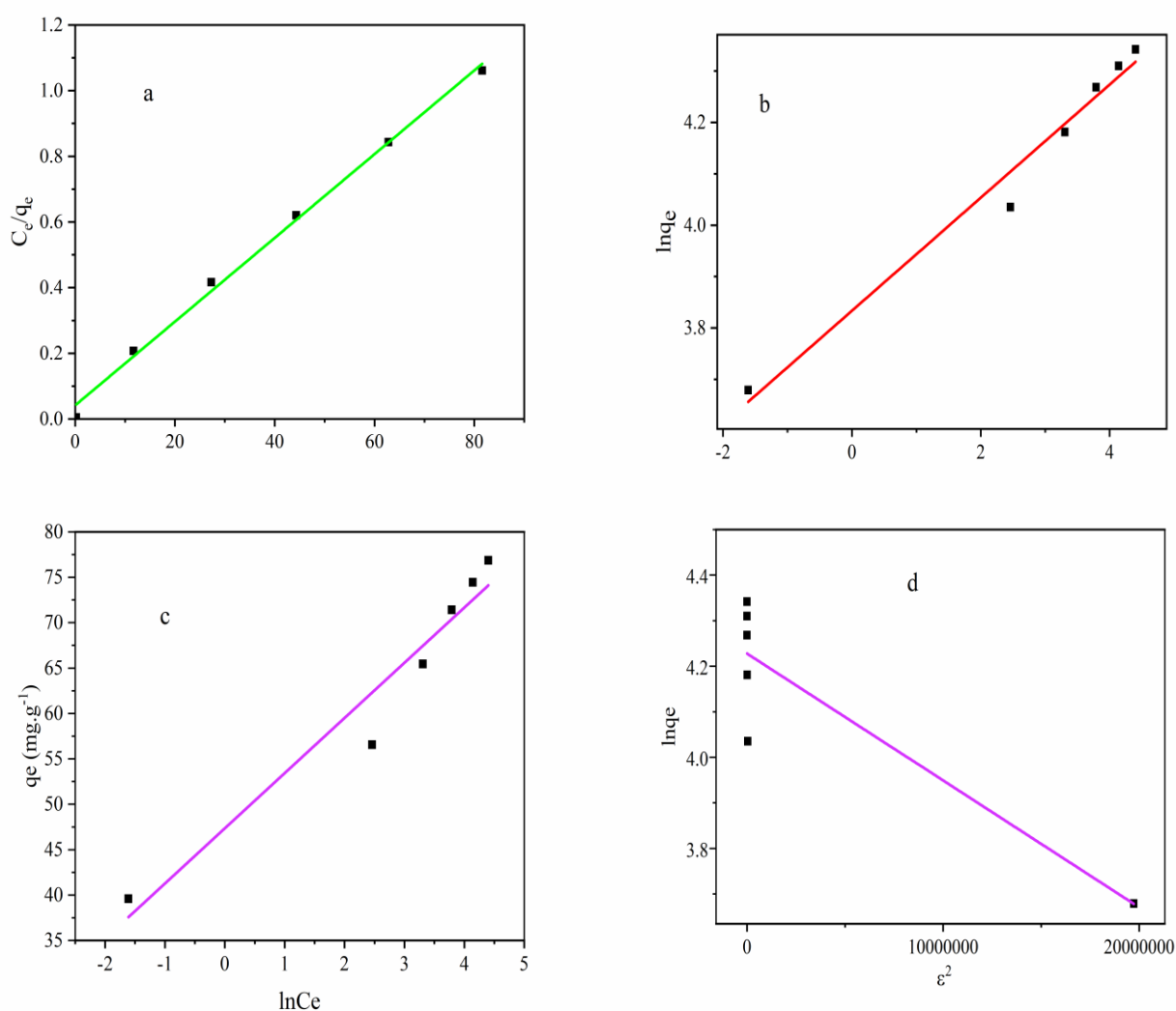| Langmuir			Freundlich		
q_m(mg g^{-1})	b	R^2	K_F	n	R^2
78.43	0.306	0.994	5.284	46.22	0.972
Temkin			Dubinin- Radushkevich (DR)		
b	K_T (L mg^{-1})	R^2	q_m	K	R^2
407.925	2765.564	0.931	68.562	$2.784*10^{-8}$	0.859

Figure **5**. Isotherm models plots for CIP adsorption (a) Langmuir, (b) Freundlich, (c) Temkin and (d) Dubinin-Radushkevich

3.5. Thermodynamics and regeneration study

Thermodynamic parameters of CIP adsorption onto MBC were calculated using Eqs. (17-19) and the results are shown in Table 6.

Table 3. Values of thermodynamic parameters for CIP adsorption onto MBC

Temperature (K)	ΔG^o (KJ mol^{-1})	ΔH^o (KJ mol^{-1})	ΔS^o (KJ mol^{-1} K^{-1})
298.15	-13.108		
308.15	-14.557	9.796	0.775
318.15	-14.629		

The obtained negative values of ΔG^o indicated the spontaneity of the sorption process (Huang et al., 2018). These results show that higher temperatures slightly favored CIP adsorption

onto the MBC. The positive values of change in enthalpy (ΔH^o) for CIP adsorption showed that the CIP sorption was an endothermic process. The change in entropy (ΔS^0) represents the adsorbent's attraction to the biochar surface.

The positive value of the entropy for CIP adsorption onto MBC indicated that the solvent molecules occupied on the surface were easily displaced by CIP molecules enhancing the adsorption capacity (Atugoda et al., 2021). In the current study, the positive values of change in entropy showed that the process of CIP adsorption was spontaneous. In conclusion, the negative Gibbs free energy and positive entropy values revealed that the CIP adsorption was favorable (Atugoda et al., 2021).

3.6. Adsorbent regeneration study

A regeneration study was conducted to evaluate the feasibility of MBC in the CIP adsorption process. Various CIP desorption solutions such as methanol, dilute HCl, 3% NaOH + methanol, and NaOH have been used in previous studies (Al et al., 2021; Balasubramani et al., 2020; Ghadiri et al., 2020) and thus selected and tested in MBC regeneration study. The CIP removal efficiency of MBC after first cycle desorption with 0.3 M NaOH, Methanol, 3% NaOH + methanol, and 0.3M HCl was 72.7, 47.09, 67.96, and 93.56%, respectively. Hence, 0.3 M HCl was used as an eluent for CIP desorption throughout the regeneration study. After 5 sequential adsorption/desorption cycles, the removal of CIP by MBC varied from 95.68% to 88.13% (reduction of 7.55%) as shown in Fig. 6. The reusability studies revealed that 88% of CIP can be removed even in the fifth cycle suggesting enhanced stability and reusability of MBC. The reusability of the MBC without significant loss in CIP removal is one of the benefits of this process regarding environmental concerns and economic feasibility.
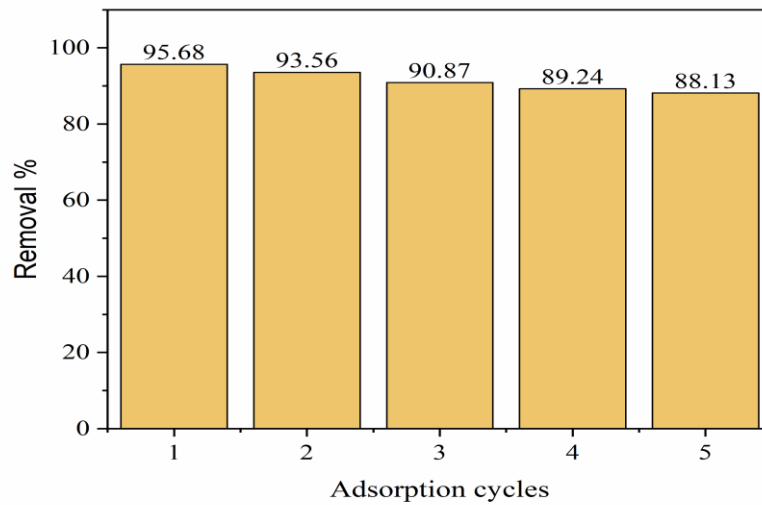
Figure 6. CIP removal efficiency of MBC per each usage cycle

3.7. Comparison of MBC with other sorbents

The maximum adsorption capacity of MBC was 78.43 mg g^{-1}. The high adsorption capacity of MBC can be ascribed to the cooperative adsorption mechanism between CIP molecules and MBC. Table 7 summarizes the CIP adsorption capacity reported for various sorbents.

Table 4. CIP removal efficiencies of various adsorbents

Adsorbent	Capacity (Maximum uptake)	Operational conditions	Isotherm and kinetics data best fit models	% CIP removal (max)	References
Azolla filiculoides activated carbon	35.14 mg g^{-1}	CIP = 10 mg L^{-1}, adsorbent dose = 2.5 g L^{-1}, contact time = 75 min	Langmuir isotherm model	99.1	(Balarak, et al., 2021)
NiO (synthesized)		adsorbent dose = 1g L^{-1},pH = 3, contact time = 90 min and 50ºC	Pseudo-second-order kinetic model	99.2	(Balarak, et al., 2021)
Amine-functionalized Mobil Composition of	164.3 mg g^{-1}	pH=7; adsorbent dose = 0.8 g L^{-1}, CIP concentration	Langmuir isotherm model and pseudo-	99.25	(Abu Rumman et al., 2021)

Adsorbent	q_{max}	Conditions	Model		Reference
Matter No. 41 (MCM–41) mesoporous silica nanoparticle		= 10 mg/L; adsorption time = 120 min, and shaking speed = 200 rpm	second-order model		
Activated carbon from lemna minor plant magnetized with iron (III) oxide magnetic nanoparticles (Fe$_3$O$_4$-ACLM)	178.7 mg g^{-1} at 50 ºC	CIP = 25 mg L^{-1}, and pH = 3, Fe$_3$O$_4$-ACLM = 0.75 g L^{-1} and contact time =75 min and 50ºC	Langmuir isotherm model	100	(Yilmaz et al., 2022)
γ-Al$_2$O$_3$ nanoparticles	-	pH = 7.5, initial CIP = 20 mg L^{-1}, adsorbent dose = 0.775 and contact time = 46.25 min	Temkin isotherm model and Pseudo-second-order kinetic model	53	(Asghar et al., 2019b)
Multi-wall carbon nanotube (MWCNTs/Al$_2$O$_3$)	41.73 mg g^{-1}	pH = 7, MWCNTs/Al$_2$O$_3$ = 1.2 g L^{-1}, Contact time = 60 min, initial CIP con = 10 mg L^{-1} and 50ºC	Langmuir isotherm model	-	(Balarak & Mckay, 2021)
Powdered activated carbon magnetized by iron (III)oxide nanoparticles (PAC@Fe$_3$O$_4$-MN)	109.833 mg g^{-1}	pH = 7, PAC@Fe$_3$O$_4$-MN dose = 1 g L^{-1}, shaking speed = 200 rpm, initial CIP = 100 mg/L, contact time = 60 min, and temperature = 298 K	Film diffusion	-	(Al et al., 2021)
Magnetic chalcogenide composite (KMS-1/L-Cysteine/Fe$_3$O$_4$ (KCF)	181.32 mg g^{-1}	pH = 6	Pseudo-second-order kinetic model	-	(Wang et al., 2018)

Adsorbent	Adsorption capacity	Conditions	Model	Removal (%)	Reference
Biochar derived from co-pyrolysis of sewage sludge and bamboo waste	62.48 mg g^{-1}	-	Pseudo-second-order, Freundlich and Langmuir model	95	(Li et al., 2020a)
Herbal residue biochar	43.668 mg g^{-1}	-	Pseudo-second-order kinetics mode		(Shang et al., 2016)
Activated carbon coated with multi-walled carbon nanotubes	-	pH = 7, contact time = 30 min, adsorbent dosage = 20 mg L^{-1}, temperature = 40 °C, and initial CIP = 20mg L^{-1}	Pseudo-second-order and Freundlich isotherm	100	(Sharifpour et al., 2020)
Magnetic Polyaniline/Graphene Oxide Based Nanocomposites	-	pH = 6, adsorbent dosage = 1 g L^{-1} and CIP = 50 mg L^{-1}, contact time = 30 min	Freundlich model and Pseudo-second-order kinetics.	97	(Kazem et al., 2018)
Low-cost hydrogel derived from agro-waste	106.038 mg g^{-1}	Adsorbent dose = 1.0 g L^{-1}, contact time = 300 min and pH = 7	Langmuir isotherm and pseudo-second-order model	-	(Nguyen et al., 2020)
Iron oxide/cellulose magnetic recyclable nanocomposite	168.03 mg g^{-1}	pH = 7, CIP concentration = 15 mg L^{-1}, adsorbent dosage = 20 mg L^{-1} and contact time = 40 min	Langmuir isotherm and pseudo-first-order kinetic model	92.01	(Azizi, 2020)
Oat hulls	83 mg g^{-1}	-	Freundlich isotherm and pseudo-second order kinetic mode	-	(Movasaghi et al., 2019)
Chitosan/biochar hydrogel beads (CBHB)	76 mg g^{-1}		Langmuir and pseudo-second order kinetics	-	(Afzal et al., 2018)

			-		
Magnesium Oxide nanoparticles (MgO)	3.46 mg g^{-1}		Langmuir adsorption isotherm and pseudo-second order kinetic model	85	(Khoshnamvand et al., 2017)
Humic acid modified hydrogel beads	154.89 mg g^{-1}	CIP concentration = 250 mg L^{-1}	Langmuir isotherm model and pseudo-second order kinetic model	-	(Zaheer et al., 2019)
Magnetic chalcogenide composite, KMS-1/L-Cystein/Fe$_3$O$_4$ (KCF)	181.32 mg g^{-1}	pH = 6	Pseudo-second-order kinetic mode and Langmuir adsorption isotherm model	-	(Wang et al., 2018)
Tannin foam immobilized with ferric ions	91.8 mg g^{-1}	pH = 7.0	Pseudo-second-order rate model Langmuir model	96.60	(Hao et al., 2021)
Surfactant Modified Sepiolite	63.84 mg g^{-1}	CIP = 10 mg L^{-1} and adsorbent dosage = 2 g L^{-1}	Pseudo-second-order model	99.1	(Balarak et al., 2020)
Modified bamboo biochar (MBC)	78.43 mg g^{-1}	adsorbent dose = 0.5 g L^{-1} CIP = 20 mg L^{-1}, pH =7.5 and contact time = 46.25 min	Pseudo-second-order rate model Langmuir model	96	This study

The use of adsorbents for the effective removal of emerging pollutants such as pharmaceutical contaminants from water is a promising technology. In this study, MBC was found to be effective for the removal of pharmaceutical contaminants such as ciprofloxacin from wastewater. Compared to others, MBC has shown higher adsorption efficiency at a relatively lower dose and less contact time for higher pollutant concentration. The adsorbent (MBC) can be synthesized from cheap and easily available raw materials promoting the circular economy. Another benefit of MBC is the simplicity of the preparation steps

compared to other adsorbents having complex synthesis steps. Moreover, MBC can be easily separated from the solution by filtration or magnetic separation. For practical water remediation applications, issues related to biochar applications in water such as the release of poly aromatic hydrocarbons (PAHs) need to be considered. In this regard, the biochar has to meet certification requirements at the commercial scale before being applied in practical water treatment processes as presented in the recent work on biochar production and certification (Osman et al., 2022). Future research works need to focus on the effect of real wastewater matrix, type of the activated biochar (granular or powder), and chemical activation after pyrolysis on the removal of CIP using MBC.

3.8. Adsorption mechanism

According to the FTIR analysis, it can be concluded that the -OH groups, C-H groups in aromatic rings, C-O alkyne, phenolic C-O bonds, and Fe-O-Fe detected on the surface of MBC may have played a significant role in the CIP adsorption process. This indicates that MBC mainly consists of aromatics, and π–π donor-acceptor interactions may occur during adsorption (Li et al., 2018). The graphitic and aromatic nature of the biochar provides electron-rich π clouds, which act as π donors. Hence, the π-π electron-donor-acceptor (EDA) interaction occurs between the biochar and electron-deficient moieties of CIP (π acceptors), enhancing the overall adsorption process. In CIP adsorption using MBC (pHpzc = 6.5), at low pH values (less than pKa_1 = 6.1), the surface functional groups and unsaturated arene groups of the MBC were protonated; thus, the π electron donor interaction with CIP was minimum. However, when pH increases from 6.1 to 8.7 (pKa_2), CIP becomes zwitterionic and capable of acting as both π donor and acceptor, promoting interactions with the biochar surface (Atugoda et al., 2021). Moreover, the –OH and –COOH groups on the MBC surface may form hydrogen bonding with moieties such as N and F-containing groups on the CIP molecules.

Furthermore, ion exchange may happen in the adsorption process. The piperazine rings of CIP molecules were positively charged (NH_2^+) in neutral or faintly acid solution, and the CIP^+ may be attracted by the polar and alkaline surface of biochar with H^+ releasing (Li et al., 2020a). Also, a complexation reaction between the Fe on the biochar and CIP molecules might be another removal mechanism (Li et al., 2020a). The Fe species probably produce hydrous oxide on the surface of biochar, and one O of the carboxylate group in the CIP molecule may bind with the hydrous oxide surface. The reason may be that the CIP molecule

forms a six-membered ring with an Fe atom through one O of the carboxylate group and keto O (Gu and Karthikeyan, 2005). The complexation reaction probably occurs between the ketone or carboxylate functional groups of zwitterions, CIP, and Fe_2O_3 of the biochar. The O atom in the carboxylic group of CIP zwitterions has been reported with a more potent ligand to interact with Fe^{3+} (Li et al., 2021). The iron species on the surface of MBC may have enhanced CIP adsorption through a complexation reaction. In fact, the adsorbent screening test revealed that bamboo biochar modified solely with ferric chloride has higher CIP removal efficiency (67.38%) than the unmodified or raw bamboo biochar (45.01%), suggesting that the iron species were involved in the CIP adsorption process. This can be supported by the disappearance of the peak assigned to the iron species on the FTIR spectra after adsorption.

4. Conclusions

In this study, the adsorption of ciprofloxacin onto MBC was optimized by response surface methodology through the central composite design approach. The results depicted that the efficiency of ciprofloxacin adsorption was reduced at both acidic and alkaline conditions due to the interplay between the pKa value of ciprofloxacin and the pH_{zpc} value of the MBC. The optimization study indicated that the adsorbent dose and contact time variables directly correlate with CIP removal efficiency, whereas the initial concentration of CIP has an inverse relationship with the removal efficiency. Statistical analysis revealed that the considered levels of MBC dose and CIP initial concentration had the most significant effects on CIP adsorption compared to other parameters studied. Based on the CCD design, the optimal operating conditions obtained for CIP adsorption onto MBC were pH (7.5), adsorbent dose (0.5 g L^{-1}), initial CIP concentration (20 mg L^{-1}), and contact time (46 min), which gave a remarkably high CIP removal of 96%. The adsorption process experimental kinetic data were well described by the Pseudo-second-order kinetic model, suggesting that the chemisorption process mainly controlled the adsorption rate. On the other hand, a kinetic study of intraparticle diffusion revealed that the adsorption rate was jointly controlled by liquid film diffusion, surface adsorption, and intra-particle diffusion.

Moreover, the isotherm study showed that Langmuir ($R^2 = 0.994$) and the Freundlich ($R^2 = 0.972$) models fit the experimental CIP adsorption data with Langmuir's superior goodness of fit. Thus, it can be deduced from these results that the adsorption of CIP onto MBC was a monolayer on a heterogeneous surface. Also, Langmuir's (R_L) and Freundlich's

(n) model parameters have indicated that CIP adsorption was favorable. Compared to the unmodified biochar, modifying bamboo with ferric chloride and alkali (potassium hydroxide) improved its surface structure and specific surface area. Hence, higher adsorption of CIP was observed for MBC than for UBC. Besides surface area increment, modification of the biochar increased biochar aromaticity. The various functional groups on the biochar surface were mainly responsible for CIP adsorption onto the MBC through π-π interaction, hydrogen bonding, ion exchange, and electrostatic interaction. Moreover, the iron species on the surface of MBC resulting from the bamboo's ferric chloride modification has probably led complexation reaction between biochar and CIP molecule. Thus, the high BET surface area (1158.05m^2/g) and the involvement of various functional groups in the adsorption process resulted in higher CIP removal by MBC from an aqueous solution. The thermodynamic study has shown that the CIP adsorption process was endothermic and spontaneous. Thus, this study revealed that MBC could be an effective adsorbent for removing ciprofloxacin from water due to its high adsorptive capacity and excellent recyclability.

Higher CIP uptake capacity and excellent reusability of the MBC could be a promising indication for practical applications. In the future, the performance of MBC in the removal of multiple pharmaceutical contaminants with different characteristics shall be addressed using fixed-bed column adsorption.

Disclosure statement

The authors declare that they have no known competing financial interests or personal relationships that could have appeared to influence the work reported in this paper.

Supplementary materials

Supplementary material associated with this article is submitted along with the article

References

Abu Rumman, G., Al-Musawi, T. J., Sillanpaa, M., & Balarak, D. (2021). Adsorption performance of an amine-functionalized MCM–41 mesoporous silica nanoparticle system for ciprofloxacin removal. *Environmental Nanotechnology, Monitoring and Management*, *16*(March), 100536. https://doi.org/10.1016/j.enmm.2021.100536

Adaobi, C., Oba, S. N., Aniagor, C. O., George, A., & Ighalo, J. O. (2021). Journal of Industrial and Engineering Chemistry Adsorption of cipro fl oxacin from water : A comprehensive review. *Journal of Industrial and Engineering Chemistry*, *93*, 57–77. https://doi.org/10.1016/j.jiec.2020.09.023

Afzal, M. Z., Sun, X. F., Liu, J., Song, C., Wang, S. G., & Javed, A. (2018). Enhancement of ciprofloxacin sorption on chitosan/biochar hydrogel beads. *Science of the Total Environment*, *639*, 560–569. https://doi.org/10.1016/j.scitotenv.2018.05.129

Al, T. J., Amir, M., Mahvi, H., Dokht, A., & Davoud, K. (2021). Effective adsorption of ciprofloxacin antibiotic using powdered activated carbon magnetized by iron (III) oxide magnetic nanoparticles. *Journal of Porous Materials*, *28*(3), 835–852. https://doi.org/10.1007/s10934-021-01039-7

Asghar, A., Nemati, O., Alidadi, H., Yazdani, M., Asghar, A., Fezabady, N., & Taghavi, M. (2019a). Optimization of ciprofloxacin adsorption from synthetic wastewaters using γ-Al 2 O 3 nanoparticles : An experimental design based on response surface methodology. *Colloid and Interface Science Communications*, *33*(July), 100212. https://doi.org/10.1016/j.colcom.2019.100212

Asghar, A., Nemati, O., Alidadi, H., Yazdani, M., Asghar, A., Fezabady, N., & Taghavi, M. (2019b). Optimization of ciprofloxacin adsorption from synthetic wastewaters using γ-Al 2 O 3 nanoparticles : An experimental design based on response surface methodology. *Colloid and Interface Science Communications*, *33*(August), 100212. https://doi.org/10.1016/j.colcom.2019.100212

Atugoda, T., Gunawardane, C., Ahmad, M., & Vithanage, M. (2021). Mechanistic interaction of ciprofloxacin on zeolite modified seaweed (Sargassum crassifolium) derived biochar: Kinetics, isotherm and thermodynamics. *Chemosphere*, *281*(November 2020), 130676. https://doi.org/10.1016/j.chemosphere.2021.130676

Azizi, A. (2020). Green synthesis of iron oxide / cellulose magnetic recyclable nanocomposite and its evaluation in ciprofloxacin removal from aqueous solutions. *Journal of the Iranian Chemical Society*, *0123456789*. https://doi.org/10.1007/s13738-020-02028-4

Balarak, D., Baniasadi, M., Lee, S., & Joon, M. (2021). *Ciprofloxacin adsorption onto Azolla filiculoides activated carbon from aqueous solutions*. *26986*, 1–10. https://doi.org/10.5004/dwt.2021.26986

Balarak, D., Baniasadi, M., Lee, S. M., & Shim, M. J. (2021). Ciprofloxacin adsorption onto azolla filiculoides activated carbon from aqueous solutions. *Desalination and Water Treatment*, *218*, 444–453. https://doi.org/10.5004/dwt.2021.26986

Balarak, D., Mahvi, A. H., Shim, M. J., & Lee, S. M. (2021). Adsorption of ciprofloxacin from aqueous solution onto synthesized NiO: Isotherm, kinetic and thermodynamic studies. *Desalination and Water Treatment*, *212*, 390–400. https://doi.org/10.5004/dwt.2021.26603

Balarak, D., & Mckay, G. (2021). Toxic / Hazardous Substances and Environmental Engineering Utilization of MWCNTs / Al 2 O 3 as adsorbent for ciprofloxacin removal : equilibrium , kinetics and thermodynamic studies. *Journal of Environmental Science and Health, Part A*, *56*(3), 324–333. https://doi.org/10.1080/10934529.2021.1873674

Balarak, D., Zafariyan, M., & Siddiqui, S. (2020). *International Journal of Lifescience and Pharma Research Investigation of Adsorptive Properties of Surfactant Modified Sepiolite for Removal of Ciprofloxacin*. *10*(3), 12–19. https://doi.org/10.22376/ijpbs/lpr.2020.10.3.P12-19

Balasubramani, K., Sivarajasekar, N., & Naushad, M. (2020). Effective adsorption of antidiabetic pharmaceutical (metformin) from aqueous medium using graphene oxide nanoparticles: Equilibrium and statistical modelling. *Journal of Molecular Liquids*, *301*, 112426. https://doi.org/10.1016/j.molliq.2019.112426

Bhattacharya, S., Das, P., Bhowal, A., & Saha, A. (2021). Thermal , Chemical and ultrasonic assisted synthesis of carbonized Biochar and its application for reducing Naproxen : Batch and Fixed bed study and subsequent optimization with response surface methodology (RSM) and artificial neural network (ANN). *Surfaces and Interfaces*,

26(July), 101378. https://doi.org/10.1016/j.surfin.2021.101378

Bilal, M., Li, C., Ren, B., & Maqbool, T. (2021). Elucidating the impacts of intermittent in-situ ozonation in a ceramic membrane bioreactor : Micropollutant removal , microbial community evolution and fouling mechanisms. *Journal of Hazardous Materials*, *402*(August 2020), 123730. https://doi.org/10.1016/j.jhazmat.2020.123730

Chang, L., Pu, Y., Jing, P., Cui, Y., Zhang, G., Xu, S., Cao, B., Guo, J., Chen, F., & Qiao, C. (2021). Magnetic core-shell MnFe2O4@TiO2 nanoparticles decorated on reduced graphene oxide as a novel adsorbent for the removal of ciprofloxacin and Cu(II) from water. *Applied Surface Science*, *541*(November), 148400. https://doi.org/10.1016/j.apsusc.2020.148400

Chen, B., Chen, Z., & Lv, S. (2011). A novel magnetic biochar efficiently sorbs organic pollutants and phosphate. *Bioresource Technology*, *102*(2), 716–723. https://doi.org/10.1016/j.biortech.2010.08.067

Chen, Y., Shi, J., Du, Q., Zhang, H., & Cui, Y. (2019). Antibiotic removal by agricultural waste biochars with different forms of iron oxide. *RSC Advances*, *9*(25), 14143–14153. https://doi.org/10.1039/c9ra01271k

Dehghan, A., Mohammadi, A. A., Yousefi, M., Najafpoor, A. A., Shams, M., & Rezania, S. (2019). Enhanced kinetic removal of ciprofloxacin onto metal-organic frameworks by sonication, process optimization and metal leaching study. *Nanomaterials*, *9*(10), 1–17. https://doi.org/10.3390/nano9101422

El-bendary, N., El-etriby, H. K., & Mahanna, H. (2021). Reuse of adsorption residuals for enhancing removal of ciprofloxacin from wastewater. *Environmental Technology*, *0*(0), 1–17. https://doi.org/10.1080/09593330.2021.1952310

Elessawy, N. A., Elnouby, M., Gouda, M. H., Hamad, H. A., Taha, N. A., Gouda, M., & Mohy, M. S. (2020). Chemosphere Cipro fl oxacin removal using magnetic fullerene nanocomposite obtained from sustainable PET bottle wastes : Adsorption process optimization , kinetics , isotherm , regeneration and recycling studies. *Chemosphere*, *239*, 124728. https://doi.org/10.1016/j.chemosphere.2019.124728

Ezekoye, O. M., Akpomie, K. G., Eze, S. I., Christian, N., Ani, J. U., Ujam, O. T., Ezekoye, O. M., Akpomie, K. G., Eze, S. I., & Christian, N. (2020). Biosorptive interaction of

alkaline modified Dialium guineense seed powders with ciprofloxacin in contaminated solution : central composite , kinetics , isotherm , thermodynamics , and desorption. *International Journal of Phytoremediation*, *0*(0), 1–10. https://doi.org/10.1080/15226514.2020.1725869

Falyouna, O., Maamoun, I., Bensaida, K., Tahara, A., Sugihara, Y., & Eljamal, O. (2022). Journal of Colloid and Interface Science Encapsulation of iron nanoparticles with magnesium hydroxide shell for remarkable removal of ciprofloxacin from contaminated water. *Journal of Colloid And Interface Science*, *605*, 813–827. https://doi.org/10.1016/j.jcis.2021.07.154

Gadipelly, C. R., Marathe, K. V, & Rathod, V. K. (2018). Effective adsorption of ciprofloxacin hydrochloride from aqueous solutions using metal-organic framework. *Separation Science and Technology*, *00*(00), 1–7. https://doi.org/10.1080/01496395.2018.1474225

Ghadiri, S. K., Alidadi, H., Nezhad, N. T., Javid, A., Roudbari, A., Talebi, S. S., Akbar, A., & Id, M. (2020). *Valorization of biomass into amine- functionalized bio graphene for efficient ciprofloxacin adsorption in water-modeling and optimization study*. 1–19. https://doi.org/10.1371/journal.pone.0231045

Gong, Y., Wang, L., Liu, J., Tang, J., & Zhao, D. (2016). Removal of aqueous perfluorooctanoic acid (PFOA) using starch-stabilized magnetite nanoparticles. *Science of the Total Environment*, *562*, 191–200. https://doi.org/10.1016/j.scitotenv.2016.03.100

Gulen, B., & Demircivi, P. (2020). Adsorption properties of fl ouroquinolone type antibiotic cipro fl oxacin into 2 : 1 dioctahedral clay structure : Box-Behnken experimental design. *Journal of Molecular Structure*, *1206*, 127659. https://doi.org/10.1016/j.molstruc.2019.127659

Hao, B., Wang, F., Huang, H., Wu, Y., Jia, S., Liao, Y., & Mao, H. (2021). Tannin foam immobilized with ferric ions for efficient removal of ciprofloxacin at low concentrations. *Journal of Hazardous Materials*, *414*(March), 125567. https://doi.org/10.1016/j.jhazmat.2021.125567

He, R., Peng, Z., Lyu, H., Huang, H., Nan, Q., & Tang, J. (2018). Synthesis and characterization of an iron-impregnated biochar for aqueous arsenic removal. *Science of*

the Total Environment, *612*, 1177–1186. https://doi.org/10.1016/j.scitotenv.2017.09.016

Huang, W., Chen, J., & Zhang, J. (2018). Removal of ciprofloxacin from aqueous solution by rabbit manure biochar. *Environmental Technology*, *0*(0), 1–28. https://doi.org/10.1080/09593330.2018.1535628

Ilurdoz, M. S. De, Sadhwani, J. J., & Reboso, J. V. (2022). Journal of Water Process Engineering Antibiotic removal processes from water & wastewater for the protection of the aquatic environment - a review. *Journal of Water Process Engineering*, *45*, 102474. https://doi.org/10.1016/j.jwpe.2021.102474

Ji, H., Wang, T., Huang, T., Lai, B., & Liu, W. (2021). Adsorptive removal of cipro fl oxacin with different dissociated species onto titanate nanotubes. *Journal of Cleaner Production*, *278*, 123924. https://doi.org/10.1016/j.jclepro.2020.123924

Karthikeyan, K. G. (2005). *Gu2005.Pdf*. *39*(23), 9166–9173.

Kaya, G. G., Aznar, E., & Deveci, H. (2021). *Low-cost silica xerogels as potential adsorbents for ciprofloxacin removal*. *22*(July). https://doi.org/10.1016/j.scp.2021.100483

Kazem, M., Nodeh, M., Soltani, S., Shahabuddin, S., & Rashidi, H. (2018). Equilibrium , Kinetic and Thermodynamic Study of Magnetic Polyaniline / Graphene Oxide Based Nanocomposites for Ciprofloxacin Removal from Water. *Journal of Inorganic and Organometallic Polymers and Materials*, *0*(0), 0. https://doi.org/10.1007/s10904-018-0782-2

Kazemi, H., Panahi, S., Dehhaghi, M., Sik, Y., Nizami, A., Khoshnevisan, B., Mussatto, S. I., Aghbashlo, M., Tabatabaei, M., & Shiung, S. (2020). A comprehensive review of engineered biochar : Production , characteristics , and environmental applications. *Journal of Cleaner Production*, *270*, 122462. https://doi.org/10.1016/j.jclepro.2020.122462

Khodadadi, M., Al-musawi, T. J., Kamranifar, M., & Saghi, M. H. (2019). *RESEARCH ARTICLE A comparative study of using barberry stem powder and ash as adsorbents for adsorption of humic acid*.

Khoshnamvand, N., Ahmadi, S., & Mostafapour, F. K. (2017). *Kinetic and Isotherm Studies*

on Ciprofloxacin an Adsorption using Magnesium Oxide Nanopartices. *7*(11), 79–83. https://doi.org/10.7324/JAPS.2017.71112

Kong, X., Liu, Y., Pi, J., Li, W., & Liao, Q. (2017). Low-cost magnetic herbal biochar : characterization and application for antibiotic removal. *Environmental Science and Pollution Research*. https://doi.org/10.1007/s11356-017-8376-z

Kumar, A., Sharma, S. K., Sharma, G., Al-Muhtaseb, A. H., Naushad, M., Ghfar, A. A., & Stadler, F. J. (2019). Wide spectral degradation of Norfloxacin by Ag@BiPO4/BiOBr/BiFeO3 nano-assembly: Elucidating the photocatalytic mechanism under different light sources. *Journal of Hazardous Materials*, *364*(August 2018), 429–440. https://doi.org/10.1016/j.jhazmat.2018.10.060

Laurent, M., Ricard, J. L., Bahain, J. J., Voinchet, P., & Rousseau, L. (2000). Datation du site Paleolithique moyen de la Butte d'Arvigny (Moissy-Cramayel, Seine-et-Marne). *Comptes Rendus de l'Academie de Sciences - Serie IIa: Sciences de La Terre et Des Planetes*, *330*(8), 581–583. https://doi.org/10.1016/S0000-0000(00)00000-0

Li, J., Pan, L., Yu, G., Li, C., Xie, S., & Wang, Y. (2021). Synthesis of an easily recyclable and safe adsorbent from sludge pyrochar for ciprofloxacin adsorption. *Environmental Research*, *192*(July 2020), 110258. https://doi.org/10.1016/j.envres.2020.110258

Li, J., Yu, G., Pan, L., Li, C., You, F., & Wang, Y. (2020a). *Ciprofloxacin adsorption by biochar derived from co-pyrolysis of sewage sludge and bamboo waste*.

Li, J., Yu, G., Pan, L., Li, C., You, F., & Wang, Y. (2020b). Ciprofloxacin adsorption by biochar derived from co-pyrolysis of sewage sludge and bamboo waste. *Environmental Science and Pollution Research*, *27*(18), 22806–22817. https://doi.org/10.1007/s11356-020-08333-y

Li, J., Yu, G., Pan, L., Li, C., You, F., Xie, S., Wang, Y., Ma, J., & Shang, X. (2018). Study of ciprofloxacin removal by biochar obtained from used tea leaves. *Journal of Environmental Sciences*, *2016*. https://doi.org/10.1016/j.jes.2017.12.024

Li, R., Wang, Z., Guo, J., Li, Y., Zhang, H., Zhu, J., & Xie, X. (2017). *Uncorrected Proof Uncorrected Proof*. 1–10. https://doi.org/10.2166/wst.2017.636

Liang, C., Zhang, X., Feng, P., Chai, H., & Huang, Y. (2018). *ZIF-67 derived hollow cobalt*

sul fi de as superior adsorbent for e ff ective adsorption removal of cipro fl oxacin antibiotics. *344*(March), 95–104. https://doi.org/10.1016/j.cej.2018.03.064

Lim, S. F., Zheng, Y. M., & Chen, J. P. (2009). Organic arsenic adsorption onto a magnetic sorbent. *Langmuir*, *25*(9), 4973–4978. https://doi.org/10.1021/la802974x

Lin, C. C., & Lee, C. Y. (2020). Adsorption of ciprofloxacin in water using Fe3O4 nanoparticles formed at low temperature and high reactant concentrations in a rotating packed bed with co-precipitation. *Materials Chemistry and Physics*, *240*(August 2019), 122049. https://doi.org/10.1016/j.matchemphys.2019.122049

Luo, K., Pang, Y., Yang, Q., Wang, D., Li, X., Wang, L., & Lei, M. (2019). Chemosphere Enhanced cipro fl oxacin removal by sludge-derived biochar : Effect of humic acid. *Chemosphere*, *231*, 495–501. https://doi.org/10.1016/j.chemosphere.2019.05.151

Ma, Y., Lu, T., Yang, L., Wu, L., Li, P., Tang, J., Chen, Y., Gao, F., Cui, S., Qi, X., & Zhang, Z. (2022). Efficient adsorptive removal of fluoroquinolone antibiotics from water by alkali and bimetallic salts co-hydrothermally modified sludge biochar. *Environmental Pollution*, *298*, 1–29. https://doi.org/10.1016/j.envpol.2022.118833

Maged, A. (2020). *Characterization of activated bentonite clay mineral and the mechanisms underlying its sorption for ciprofloxacin from aqueous solution*. 32980–32997.

Mahmoud, M. E., Saad, S. R., El-Ghanam, A. M., & Mohamed, R. H. A. (2021). Developed magnetic Fe3O4–MoO3-AC nanocomposite for effective removal of ciprofloxacin from water. *Materials Chemistry and Physics*, *257*(June 2020), 123454. https://doi.org/10.1016/j.matchemphys.2020.123454

Mi, X., Li, Y., Ning, X., Jia, J., Wang, H., Xia, Y., Zhan, S., Li, Y., Ning, X., Jia, J., Wang, H., Xia, Y., Sun, Y., & Zhan, S. (2018). *Electro-Fenton degradation of ciprofloxacin with highly ordered mesoporous MnCo 2 O 4 -CF cathode : enhanced redox capacity and accelerated electron transfer*. https://doi.org/10.1016/j.cej.2018.10.047

Mian, M., Liu, G., Yousaf, B., Fu, B., Ullah, H., Ubaid, M., Abbas, Q., Ahmed, M., Munir, M., & Ruijia, L. (2018). Chemosphere Simultaneous functionalization and magnetization of biochar via NH 3 ambiance pyrolysis for ef fi cient removal of Cr (VI). *Chemosphere*, *208*, 712–721. https://doi.org/10.1016/j.chemosphere.2018.06.021

Mohammed, S. J., M-ridha, M. J., Abed, K. M., & Amal, A. M. (2021). Removal of levofloxacin and ciprofloxacin from aqueous solutions and an economic evaluation using the electrocoagulation process . *International Journal of Environmental Analytical Chemistry*, *00*(00), 1–19. https://doi.org/10.1080/03067319.2021.1913733

Movasaghi, Z., Yan, B., & Niu, C. (2019). Industrial Crops & Products Adsorption of ciprofloxacin from water by pretreated oat hulls : Equilibrium , kinetic , and thermodynamic studies. *Industrial Crops & Products*, *127*(October 2018), 237–250. https://doi.org/10.1016/j.indcrop.2018.10.051

Nazraz, M., Yamini, Y., & Asiabi, H. (2019). *Chitosan-based sorbent for efficient removal and extraction of ciprofloxacin and norfloxacin from aqueous solutions*.

Nemati, O., Asghar, A., Yazdani, M., & Taghavi, M. (2019). Journal of Water Process Engineering Catalytic ozonation of cipro fl oxacin using γ -Al 2 O 3 nanoparticles in synthetic and real wastewaters. *Journal of Water Process Engineering*, *32*(June), 100894. https://doi.org/10.1016/j.jwpe.2019.100894

Ngeno, Emily C, Shikuku, V. O., Orata, F., Baraza, L. D., & Kimosop, S. J. (2019). *Caffeine and Ciprofloxacin Adsorption from Water onto Clinoptilolite : Linear Isotherms , Kinetics , Thermodynamic and Mechanistic Studies*. 136–142.

Ngeno, Emily Chelangat, Orata, F., Baraza, L. D., Shikuku, V. O., & Jemutai, S. (2016). *Adsorption of Caffeine and Ciprofloxacin onto Pyrolitically Derived Water Hyacinth Biochar: Isothermal, Kinetic and Thermodynamic Studies*. *10*, 185–194. https://doi.org/10.17265/1934-7375/2016.04.006

Nguyen, H. T., Phuong, V. N., & Van, T. N. (2020). Environmental Technology & Innovation Low-cost hydrogel derived from agro-waste for veterinary antibiotic removal : Optimization , kinetics , and toxicity evaluation. *Environmental Technology & Innovation*, *20*, 101098. https://doi.org/10.1016/j.eti.2020.101098

Osman, A. I., Connor, E. O., Mcspadden, G., Abu-dahrieh, J. K., Farrell, C., Al-muhtaseb, A. H., Harrison, J., & Rooney, D. W. (2019). *Upcycling brewer ' s spent grain waste into activated carbon and carbon nanotubes for energy and other applications via two-stage activation*. *July*. https://doi.org/10.1002/jctb.6220

Osman, A. I., Farrell, C., Al-Muhtaseb, A. H., Harrison, J., & Rooney, D. W. (2020). The

production and application of carbon nanomaterials from high alkali silicate herbaceous biomass. *Scientific Reports*, *10*(1), 1–13. https://doi.org/10.1038/s41598-020-59481-7

Osman, A. I., Fawzy, S., Farghali, M., El, M., Ahmed, A., & Rooney, D. W. (2022). Biochar for agronomy , animal farming , anaerobic digestion , composting , water treatment , soil remediation , construction , energy storage , and carbon sequestration : a review. In *Environmental Chemistry Letters* (Issue 0123456789). Springer International Publishing. https://doi.org/10.1007/s10311-022-01424-x

Peña, A. M. C.-, Ibanez, J. G., & Vasquez-medrano, R. (2012). *Determination of the Point of Zero Charge for Electrocoagulation Precipitates from an Iron Anode*. *7*, 6142–6153.

Peng, H., Guo, J., Qiu, H., Wang, C., Zhang, C., Hao, Z., Rao, Y., & Gong, Y. (2021). Efficient removal of cr (Vi) with biochar and optimized parameters by response surface methodology. *Processes*, *9*(5). https://doi.org/10.3390/pr9050889

Peng, X., Hu, F., Zhang, T., Qiu, F., & Dai, H. (2018). Amine-functionalized magnetic bamboo-based activated carbon adsorptive removal of ciprofloxacin and norfloxacin: A batch and fixed-bed column study. *Bioresource Technology*, *249*, 924–934. https://doi.org/10.1016/j.biortech.2017.10.095

Rajapaksha, A. U., Shashikala, K., Premarathna, D., Gunarathne, V., Ahmed, A., & Vithanage, M. (2019). 9. Sorptive removal of pharmaceutical and personal care products from water and wastewater. In *Pharmaceuticals and Personal Care Products: Waste Management and Treatment Technology*. Elsevier Inc. https://doi.org/10.1016/B978-0-12-816189-0.00009-3

Rajiv, P., Mengelizadeh, N., & Mckay, G. (2021). Photocatalytic degradation of ciprofloxacin with Fe 2 O 3 nanoparticles loaded on graphitic carbon nitride : mineralisation , degradation mechanism and toxicity assessment. *International Journal of Environmental Analytical Chemistry*, *00*(00), 1–15. https://doi.org/10.1080/03067319.2021.1890059

Reguyal, F., Sarmah, A. K., & Gao, W. (2016). Synthesis of magnetic biochar from pine sawdust via oxidative hydrolysis of FeCl2 for the removal sulfamethoxazole from aqueous solution. *Journal of Hazardous Materials*. https://doi.org/10.1016/j.jhazmat.2016.10.006

Río-gamero, B. Del, Alonso, J. J. S., Kori, N. El, & Meli, N. (2018). *Removal of cipro fl oxacin from seawater by reverse osmosis. 217.* https://doi.org/10.1016/j.jenvman.2018.03.108

Sadiq, H., Sher, F., Sehar, S., Lima, E. C., Zhang, S., Iqbal, H. M. N., Zafar, F., & Nuhanović, M. (2021). Green synthesis of ZnO nanoparticles from Syzygium Cumini leaves extract with robust photocatalysis applications. *Journal of Molecular Liquids*, *335*. https://doi.org/10.1016/j.molliq.2021.116567

Shang, J. G., He, X. R. K. L. L., & Liao, W. H. L. Q. J. H. (2016). *Low-cost biochar derived from herbal residue : characterization and application for ciprofloxacin adsorption.* https://doi.org/10.1007/s13762-016-1075-3

Sharifpour, N., Mohammadi, F., Goshtasb, M., & Mohammad, M. (2020). Evaluation of the activated carbon coated with multiwalled carbon nanotubes in removal of ciprofloxacin from aqueous solutions. *Applied Water Science*, *10*(6), 1–17. https://doi.org/10.1007/s13201-020-01229-9

Sharma, G., Gupta, V. K., Agarwal, S., Bhogal, S., Naushad, M., Kumar, A., & Stadler, F. J. (2018). Fabrication and characterization of trimetallic nano-photocatalyst for remediation of ampicillin antibiotic. *Journal of Molecular Liquids*, *260*(2017), 342–350. https://doi.org/10.1016/j.molliq.2018.03.059

Soares, S. F., João, M., Ferro, M., Amorim, C. O., Amaral, J. S., Trindade, T., & Daniel-da-silva, A. L. (2019). International Journal of Biological Macromolecules Magnetic nanosorbents with siliceous hybrid shells of alginic acid and carrageenan for removal of ciprofloxacin. *International Journal of Biological Macromolecules*, *139*, 827–841. https://doi.org/10.1016/j.ijbiomac.2019.08.030

Stylianou, M., Christou, A., Michael, C., Agapiou, A., Papanastasiou, P., & Fatta-kassinos, D. (2021). Journal of Environmental Chemical Engineering Adsorption and removal of seven antibiotic compounds present in water with the use of biochar derived from the pyrolysis of organic waste feedstocks. *Journal of Environmental Chemical Engineering*, *9*(5), 105868. https://doi.org/10.1016/j.jece.2021.105868

Tawfik, A., Alalm, M. G., Awad, H. M., Islam, M., Qyyum, M. A., Al-Muhtaseb, A. H., Osman, A. I., & Lee, M. (2022). Solar photo-oxidation of recalcitrant industrial

wastewater: a review. *Environmental Chemistry Letters*, *20*(3), 1839–1862. https://doi.org/10.1007/s10311-022-01390-4

Wan, J., & Li, Z. (2019). Adsorption properties and mechanisms of novel biomaterials from banyan aerial roots via simple modification for ciprofloxacin removal School of Environment and Energy , South China University of Technology , Guangzhou Sino-Singapore International Joint Re. *Science of the Total Environment*, 134630. https://doi.org/10.1016/j.scitotenv.2019.134630

Wang, Y., Gupta, K., Li, J., Yuan, B., & Yang, J. E. (2018). Novel chalcogenide based magnetic adsorbent KMS-1 / L-Cystein / Fe 3 O 4 for the facile removal of cipro fl oxacin from aqueous solution. *Colloids and Surfaces A*, *538*(November 2017), 378–386. https://doi.org/10.1016/j.colsurfa.2017.11.016

Wang, Y. X., Ngo, H. H., & Guo, W. S. (2015). *Science of the Total Environment Preparation of a speci fi c bamboo based activated carbon and its application for cipro fl oxacin removal Total-V. 533*, 32–39. https://doi.org/10.1016/j.scitotenv.2015.06.087

Wu, Q., Li, Z., Hong, H., Yin, K., & Tie, L. (2010). *Applied Clay Science Adsorption and intercalation of cipro fl oxacin on montmorillonite. 50*, 204–211. https://doi.org/10.1016/j.clay.2010.08.001

Yilmaz, M., Al, T. J., Morteza, M., Dokht, A., & Marziyeh, K. (2022). Synthesis of activated carbon from Lemna minor plant and magnetized with iron (III) oxide magnetic nanoparticles and its application in removal of Ciprofloxacin. *Biomass Conversion and Biorefinery*, *Iii*. https://doi.org/10.1007/s13399-021-02279-y

Yousefi, M., Gholami, M., Oskoei, V., & Akbar, A. (2021). Journal of Environmental Chemical Engineering Comparison of LSSVM and RSM in simulating the removal of ciprofloxacin from aqueous solutions using magnetization of functionalized multi-walled carbon nanotubes : Process optimization using GA and RSM techniq. *Journal of Environmental Chemical Engineering*, *9*(4), 105677. https://doi.org/10.1016/j.jece.2021.105677

Yu, F., Sun, Y., Yang, M., & Ma, J. (2019). Adsorption mechanism and effect of moisture contents on ciprofloxacin removal by three-dimensional porous graphene hydrogel. *Journal of Hazardous Materials*, *374*(March), 195–202.

https://doi.org/10.1016/j.jhazmat.2019.04.021

Zaheer, M., Yue, R., Sun, X., Song, C., & Wang, S. (2019). Journal of Colloid and Interface Science Enhanced removal of ciprofloxacin using humic acid modified hydrogel beads. *Journal of Colloid And Interface Science*, *543*, 76–83. https://doi.org/10.1016/j.jcis.2019.01.083

Zahoor, M., Ullah, A., Alam, S., Muhammad, M., Setyobudi, R. H., Zekker, I., & Sohail, A. (2022). *Novel Magnetite Nanocomposites (Fe 3 O 4 / C) for Efficient Immobilization of Ciprofloxacin from Aqueous Solutions through Adsorption Pretreatment and Membrane Processes*.

Zhang, B., Han, X., Gu, P., Fang, S., & Bai, J. (2017). Response surface methodology approach for optimization of cipro fl oxacin adsorption using activated carbon derived from the residue of desilicated rice husk. *Journal of Molecular Liquids*, *238*, 316–325. https://doi.org/10.1016/j.molliq.2017.04.022

Zhao, H., Cao, Z., Li, J., & Lang, Y. (2018). *Adsorptive Removal of Ciprofloxacin by Ferric Chloride Modified Biochar*. *Iweg*, 56–61.

Zheng, X., He, X., Peng, H., Wen, J., & Lv, S. (2021). Bioresource Technology Efficient adsorption of ciprofloxacin using Ga 2 S 3 / S-modified biochar via the high-temperature sulfurization. *Bioresource Technology*, *334*(March), 125238. https://doi.org/10.1016/j.biortech.2021.125238